Multi-instrument observations from Svalbard of a traveling convection vortex, electromagnetic ion cyclotron wave burst, and proton precipitation associated with a bow shock instability

M. J. Engebretson,[1] T. K. Yeoman,[2] K. Oksavik,[3,4] F. Søraas,[3,4] F. Sigernes,[5] J. I. Moen,[5,6]
M. G. Johnsen,[7] V. A. Pilipenko,[1,8] J. L. Posch,[1] M. R. Lessard,[9] B. Lavraud,[10,11]
M. D. Hartinger,[12] L. B. N. Clausen,[6,13] T. Raita,[14] and C. Stolle[15]

[1]   An isolated burst of 0.35 Hz electromagnetic ion cyclotron (EMIC) waves was observed at four sites on Svalbard from 0947 to 0954 UT 2 January 2011, roughly 1 h after local noon. This burst was associated with one of a series of ~50 nT magnetic impulses observed at the northernmost stations of the IMAGE magnetometer array. Hankasalmi SuperDARN radar data showed a west-to-east (antisunward) propagating vortical ionospheric flow in a region of high spectral width ~ 1–$2°$ north of Svalbard, confirming that this magnetic impulse was the signature of a traveling convection vortex. Ground-based observations of the H_α line at Longyearbyen indicated proton precipitation at the same time as the EMIC wave burst, and NOAA-19, which passed over the west coast of Svalbard between 0951 and 0952, observed a clear enhancement of ring current protons at the same latitude. Electron precipitation from this same satellite indicated that the EMIC burst was located on closed field lines, but near to the polar cap boundary. We believe these are the first simultaneous observations of EMIC waves and precipitating energetic protons so near to the boundary of the dayside magnetosphere. Although several spacecraft upstream of Earth observed a steady solar wind and predominantly radial interplanetary magnetic field orientation before and during this event, data from Geotail (near the morning bow shock) showed large reorientations of the interplanetary magnetic field and substantial decreases in ion density several minutes before it, and data from Cluster (near the afternoon bow shock) showed an outward excursion of the bow shock simultaneous with it. These upstream perturbations suggest that a spontaneous hot flow anomaly, a bow shock related instability, may have been responsible for triggering this event, but do not provide enough information to fully characterize that instability.

Citation: Engebretson, M. J., et al. (2013), Multi-instrument observations from Svalbard of a traveling convection vortex, electromagnetic ion cyclotron wave burst, and proton precipitation associated with a bow shock instability, *J. Geophys. Res. Space Physics*, *118*, 2975–2997, doi:10.1002/jgra.50291.

1.   Introduction

[2] Traveling convection vortices, or TCVs, occur as solitary quasi-sinusoidal transients near the dayside magnetopause with frequencies ~2–5 mHz. They were first reported by *Friis-Christensen et al.* [1988] and *Glassmeier et al.* [1989] in ground-based magnetometer data at near-cusp latitudes.

[3] Various drivers for TCVs have been suggested, including flux transfer events, solar wind pressure pulses, and instabilities in the ion foreshock just upstream of Earth's

---

[1]Department of Physics, Augsburg College, Minneapolis, Minnesota, USA.
[2]Department of Physics and Astronomy, University of Leicester, Leicester, UK.
[3]Department of Physics and Technology, University of Bergen, Bergen, Norway.
[4]Birkeland Centre for Space Science, Bergen, Norway.
[5]Department of Geophysics, University Centre in Svalbard, Longyearbyen, Norway.
[6]Department of Physics, University of Oslo, Oslo, Norway.

Corresponding author: M. J. Engebretson, Department of Physics, Augsburg College, Minneapolis, MN 55454 USA. (engebret@augsburg.edu)

[7]Tromsø Geophysical Observatory, University of Tromsø, Tromsø, Norway.
[8]Space Research Institute, Moscow, Russia.
[9]Department of Physics, University of New Hampshire, Durham, New Hampshire, USA.
[10]Institut de Recherche en Astrophysique et Planétologie, Université de Toulouse (UPS), France.
[11]Centre National de la Recherce Scientifique, Toulouse, France.
[12]Department of Atmospheric, Oceanic, and Space Sciences, University of Michigan, Ann Arbor, Michigan, USA.
[13]Technische Universität Braunschweig, Braunschweig, Germany.
[14]Sodankylä Geophysical Observatory, University of Oulu, Finland.
[15]Technical University of Denmark, DTU Space, Copenhagen, Denmark.
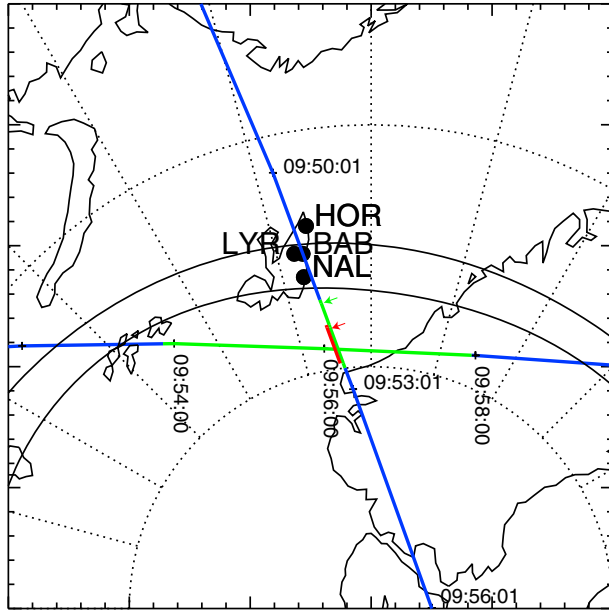
Figure 1. Map of Svalbard, northern Greenland, and Scandinavia in magnetic latitude-magnetic local time coordinates at 0950 UT, showing the locations of the search coil magnetometers at Ny Ålesund (NAL), Longyearbyen (LYR), Barentsburg (BAB), and Hornsund (HOR) and a typical auroral oval location. Concentric circles show magnetic latitude at 10° increments, and radial dotted lines local time at 1 h increments. Also shown in this figure are the ground tracks of NOAA 19 (moving mostly northward) and DMSP F17 (moving mostly westward), both of which passed near Svalbard during the TCV and EMIC wave burst on 2 January 2011. The colored tracks and arrows are described in section 5.

bow shock [*Konik et al.*, 1994; *Lühr and Blawert*, 1994; *Sibeck et al.*, 1999; *Murr and Hughes*, 2003; *Omidi et al.*, 2010]. Each of these mechanisms can generate changes in dynamic pressure at the dayside magnetospheric boundary, resulting in transient magnetic field variations and field-aligned currents. Detailed descriptions and comparisons of

several of these mechanisms are given by *Cowley* [2000] and *Lockwood et al.* [1990]. There has been renewed interest in TCVs in recent years because of the availability of multipoint satellite observations upstream of the magnetopause and bow shock, including prominent contributions from the five Time History of Events and Macroscale Interactions during Substorms (THEMIS) spacecraft [e.g., *Eastwood et al.*, 2008; *Jacobsen et al.*, 2009; *Turner et al.*, 2011; *Archer et al.*, 2012].

[4] *Arnoldy et al.* [1988, 1996] were the first to note that bursts of Pc 1–2 pulsations (0.2–1.0 Hz) were often associated with long-period magnetic transient events in the outer dayside magnetosphere. By correlating magnetopause displacements (detected by the AMPTE CCE satellite) and bursts at South Pole Station, Antarctica, *Anderson et al.* [1996] observed that Pc 1 bursts can be stimulated by compressions of the dayside magnetosphere, and can have a source region that extends 1 to 2 h azimuthally and 1 to 2 R_E radially earthward of the low-latitude boundary layer. A recent statistical study by *Posch et al.* [2011] found that, of the long-period transient events observed in cusp-latitude ground data within ± 3 h of local noon in 2008–2009, roughly 25% were accompanied by nearly simultaneous Pc 1 wave bursts at the same or nearby stations.

[5] Other observational and theoretical studies of Pc 1 wave events triggered by dayside magnetospheric compressions include those by *Olson and Lee* [1983], *Kangas et al.* [1986], *Ishida et al.* [1987], *Anderson and Hamilton* [1993], *Kangas et al.* [1998], *Engebretson et al.* [2002], *Arnoldy et al.* [2005], *Posch et al.* [2010], *Clausen et al.* [2011], and *Usanova et al.* [2008, 2010, 2012] . Several of these studies showed that these events are not limited to near-cusp latitudes, but can occur even inside the plasmapause.

[6] Other studies have identified means by which ion distributions in the dayside magnetosphere can become sufficiently anisotropic (with perpendicular temperature exceeding parallel temperature) to reach the threshold of the electromagnetic ion cyclotron (EMIC) wave instability, which is commonly considered to be the source of magnetospheric Pc 1 waves. *Usanova et al.* [2012] recently reviewed three possible mechanisms that can lead to anisotropic proton distributions in the dayside outer magnetosphere:

Table 1. Locations of the Search Coil Magnetometers Used in This Study[a]

Station		Geog. Lat	Geog. Long.	L Shell	Corr. Geom. Lat.	Corr. Geom. Long.	UT of Noon MLT
NAL	Ny Ålesund	78.93°N	11.93°E	Polar Cap	76.44°N	109.69°E	9:02
LYR	Longyearbyen	78.15°N	16.03°E	Polar Cap	75.43°N	110.78°E	8:58
BAB	Barentsburg	78.08°N	14.20°E	Polar Cap	75.48°N	109.39°E	9:03
HOR	Hornsund	77.01°N	15.55°E	14.0	74.37°N	108.32°E	9:07
SPA	South Pole	90°S	—	13.9	74.34°S	18.68°E	15:37
IQA	Iqaluit	63.75°N	291.48°E	10.5	71.86°N	14.85°E	16:17
STF	Sondrestromfjord	67.02°N	309.28°E	11.0	72.32°N	39.98°E	14:45
KIL	Kilpisjärvi	69.02°N	20.86°E	6.2	66.05°N	103.25°E	9:25
IVA	Ivalo	68.55°N	27.28°E	5.8	65.30°N	108.10°E	9:05
SOD	Sodankyla	67.42°N	26.39°E	5.4	64.18°N	106.67°E	9:11
ROV	Rovaniemi	66.78°N	25.94°E	5.1	63.55°N	105.93°E	9:13
OUL	Oulu	65.0°N	25.5°E	4.5	61.73°N	104.62°E	9:19
NUR	Nurmijärvi	60.51°N	24.65°E	3.4	57.06°N	101.96°E	9:29

[a]Corrected geomagnetic coordinates and UT of local magnetic noon (MLT) have been computed for epoch 2011 and an altitude of 100 km using the NSSDC modelweb facility (http://nssdc.gsfc.nasa.gov/space/cgm/cgm.html).

Table 2. Peak-to-Peak Wave Amplitudes and Signal-to-Noise Ratios for Search Coil Magnetometer Data Filtered Between 0.1 and 0.6 Hz During the Wave Event Near 0952 UT

Station	Bx (nT/s)	By (nT/s)	Bx (nT)	By (nT)	S/N X	S/N Y
Ny Ålesund	1.6	1.2	0.7	0.5	40	30
Longyearbyen	1.8	2.8	0.8	1.3	30	47
Barentsburg	1.6 [a]	2.4 [a]	0.7 [a]	1.1 [a]	36	50
Hornsund	1.8	1.4	0.8	0.6	30	23
Sondrestromfjord	0.04	0.02	0.02	0.01	1.3	1
Kilpisjarvi					3	3.2
Ivalo					2.2	2.3
Sodankylä					2	2.2
Rovaniemi					2	2
Oulu					1.5	1.2

[a]Determined relative to others; calibration not yet known.

(1) drift shell splitting [e.g., *Sibeck et al.*, 1987]; (2) the presence of Shabansky orbits (mirroring at high latitudes rather than at the equator) causing depletion of particles with low pitch angles near the equator [*McCollough et al.*, 2012]; and (3) adiabatic heating during short-term magnetospheric compressions. The third of these mechanisms is considered to act on ion distributions made marginally unstable by the first two methods, thus causing bursts of Pc 1 waves in association with these compressions. The effectiveness of transient compressions of the dayside magnetosphere to increase the temperature anisotropy of ions can be expressed in terms of perpendicular heating by an increase of |B| (betatron acceleration) exceeding parallel heating by field line shortening (Fermi acceleration). This is analogous to the action of these two acceleration mechanisms in the night-side magnetosphere, which also is observed to produce more "pancake" pitch angle distributions of electrons injected from the midtail during substorm dipolarizations [*Smets et al.*, 1999; *Wu et al.*, 2006].

[7] Because the free energy needed to drive EMIC waves comes from the temperature anisotropy of the distribution of kiloelectron-volt plasma sheet ions and/or tens of kiloelectron-volt ring current ions, and causes them to scatter in pitch angle, one consequence of their generation is the precipitation of protons into the ionosphere. *Yahnina et al.* [2000] found at subauroral latitudes that localized proton precipitation (>30 keV) measured by low-altitude NOAA satellites was related to the occurrence of Pc1 waves on the ground, and *Usanova et al.* [2010] reported NOAA 17 observations of precipitating protons with energies > 30 keV simultaneous with compression-related Pc1 waves observed both on the ground and at the Cluster spacecraft near $L \sim 5$. Localized subauroral proton auroras associated with Pc1 waves were also observed by the IMAGE satellite [*Immel et al.*, 2005; *Yahnin et al.*, 2007], and *Sakaguchi et al.* [2007, 2008] found a one-to-one correspondence between
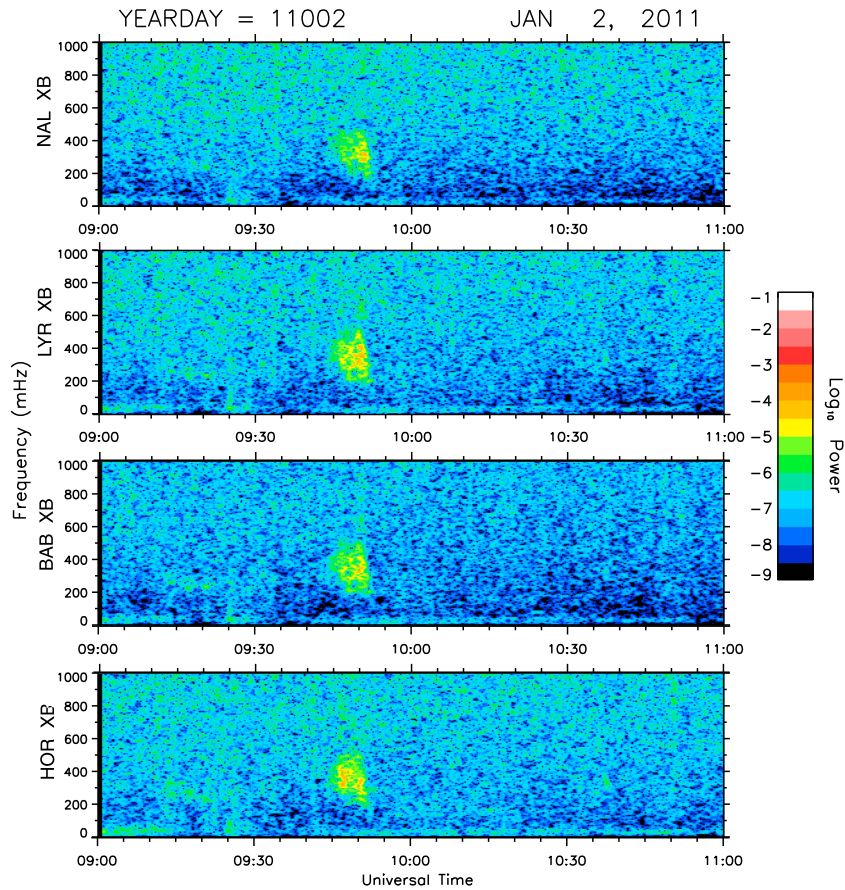
Figure 2. Fourier spectrogram of the X (north-south) component of search coil magnetometer data from four stations in Svalbard (Ny Ålesund, Longyearbyen, Barentsburg, and Hornsund) from 0900 to 1100 UT 2 January 2011.

Table 3. Locations of the IMAGE and Western Greenland Fluxgate Magnetometers Used in This Study[a]

| Station		Geog. Lat	Geog. Long.	L Shell	Corr. Geom. Lat.	Corr. Geom. Long.	UT of Noon MLT
				IMAGE			
NAL	Ny Ålesund	78.92°N	11.95°E	Polar cap	76.43	109.68	9.04
LYR	Longyearbyen	78.20°N	15.82°E	Polar Cap	75.49	110.73	8.97
HOR	Hornsund	77.00°N	15.60°E	14.0	74.35	108.34	9.12
HOP	Hopen Island	76.51°N	25.01°E	12.3	73.33	114.20	8.72
BJN	Bear Island	74.50°N	19.20°E	10.25	71.65	107.08	9.17
NOR	Nordkapp	71.09°N	25.79º E	7.2	67.93	108.78	9.05
MAS	Masi	69.46°N	23.70°E	6.3	66.37	105.85	9.24
MUO	Muonio	68.02°N	23.53°E	5.65	64.90	104.70	9.31
PEL	Pello	66.90°N	24.08°E	5.2	63.73	104.47	9.32
				Western Greenland			
THL	Qaanaaq	77.47°N	290.77°E	Polar cap	84.57	27.65	15.33
KUV	Kullorsuaq	74.57°N	302.82°E	Polar cap	80.51	40.52	14.41
UPN	Upernavik	72.78°N	303.85°E	Polar cap	78.74	38.85	14.53
UMQ	Umanaq	70.68°N	307.87°E	Polar cap	76.16	41.33	14.34
GDH	Qeqertarsuaq	69.25°N	306.47°E	15.15	75.00	38.18	14.57
STF	Kangerlussuaq	67.02°N	309.28°E	11.0	72.32	39.98	14.45
SKT	Maniitsoq	65.42°N	307.10°E	9.7	71.11	36.39	14.71
GHB	Nuuk	64.17°N	308.27°E	8.4	69.67	37.07	14.66
FHB	Paamiut	62.00°N	310.32°E	6.7	67.11	38.37	14.56

[a]Corrected geomagnetic coordinates and UT of local magnetic noon (MLT) have been computed for epoch 2011 and an altitude of 100 km using the NSSDC modelweb facility (http://nssdc.gsfc.nasa.gov/space/cgm/cgm.html).

the isolated proton auroras observed by a ground all-sky camera and the Pc1 waves observed by a ground induction magnetometer. *Yahnin and Yahnina* [2007] reviewed recent studies of simultaneous EMIC waves and proton precipitation, but focused on regions associated with the plasmapause or plasmaspheric plumes. The observations reported in this manuscript are from a very different region, on field lines that map close to the magnetospheric boundary: ~1 h after local magnetic noon, and from ~70° MLAT to the latitude of the open-closed boundary.

[8] *Sandanger et al.* [2007] reviewed observations of NOAA-12 MEPED data showing enhancements in precipitating and locally mirroring 30–80 keV protons. They found that EMIC wave-particle interactions that were effective in scattering relativistic electrons were not restricted to a narrow region at/or inside the plasmapause, and could be observed at all local times, not just the evening/noon MLT sector. They noted, however, that EMIC waves at the plasmapause and/or in plumes might be very strong and would thus be easier to observe.

[9] The TCV and EMIC burst event reported here is of interest both because of the availability of data from many additional sources, both space- and ground-based, and because we believe this is the first TCV / EMIC burst event for which
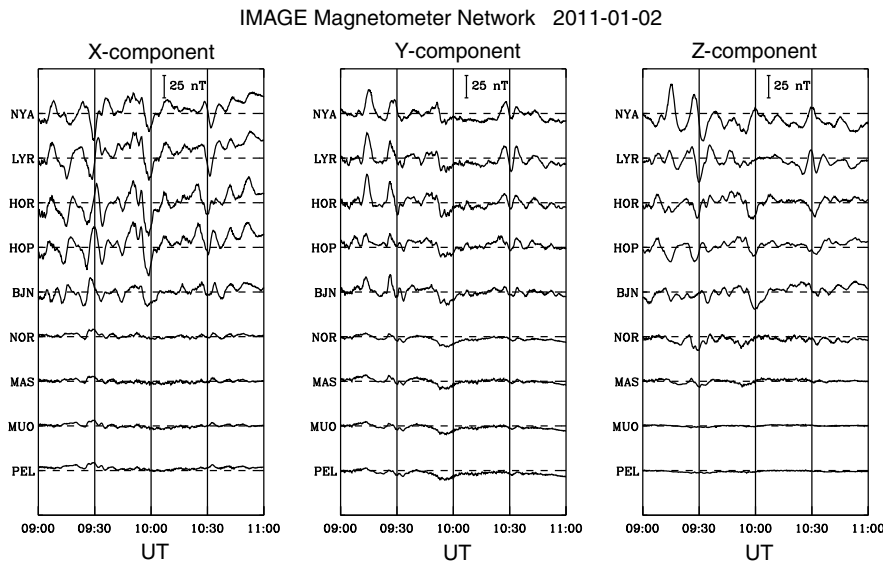
Figure 3. Stacked plot of 10 s geomagnetic component data from a chain of stations in the IMAGE magnetometer network listed in Table 3, arranged in order of decreasing magnetic latitude, from 0900 to 1100 UT 2 January 2011.
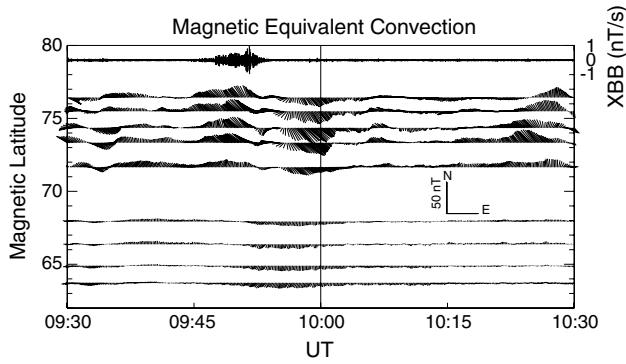
Figure 4. The upper trace shows the north-south (X) component of Longyearbyen search coil magnetometer data, bandpass filtered in the range from 0.1 to 0.5 Hz, from 0930 to 1030 UT 2 January 2011. All other traces show the magnetic equivalent convection as a time series of vectors over the same time period, based on 10 s geomagnetic component data from the same stations in the IMAGE magnetometer network shown in Figure 3, arranged in order of decreasing magnetic latitude.

observations of precipitating protons are available from both the ground and from space. These strongly suggest that localized proton precipitation associated with EMIC waves can be generated very near the outer boundary of the dayside magnetosphere. Section 2 describes the ground-based magnetometer observations that led to the identification of this event. Section 3 presents the SuperDARN radar data that show it to have been a TCV, and combined SuperDARN and DMSP data that confirm the location of the radar signature to be near the open-closed magnetic field line boundary. In section 4 we present evidence that this TCV event was also observed by magnetometers and radars at similar latitudes in western Greenland at prenoon local times, although the longitudinal extent and variation of the TCV event will not be discussed in detail. Section 5 discusses both ground-based and space-based observations of proton and electron precipitation associated with this event, and section 6 presents observations from spacecraft upstream from Earth that indicate that a recently identified bow shock related instability, a spontaneous hot flow anomaly [*Omidi et al.*, 2013; *H. Zhang et al.,* Spontaneous hot flow anomalies at quasi-parallel shocks, 1, Observations, submitted to *Journal of Geophysical Research*, 2012], was the probable source of the transient magnetospheric compression that initiated the TCV and associated EMIC wave burst.

2. Ground-Based Magnetometer Observations on Svalbard

[10] Observations of Pc 1–2 waves presented here were obtained from a closely spaced array of four search coil (pulsation) magnetometers on Svalbard (Figure 1 and Table 1). Three of these (Ny Ålesund (NAL), Longyearbyen (LYR), Hornsund (HOR)) are operated by Augsburg College and the University of New Hampshire [*Engebretson et al.*, 2009]. The Barentsburg (BAB) instrument is operated by the Polar Geophysical Institute, Apatity, Russia. Data from

the Finnish pulsation magnetometer chain and from Augsburg-UNH pulsation magnetometers at Sondrestromfjord (Kangerlussuaq), Greenland, Iqaluit, Canada, and South Pole Station, Antarctica were also examined for signatures of these waves, and showed considerably weaker signals (Table 1).

[11] Figure 2 shows a frequency-time Fourier spectrogram of differenced ULF wave power in the X (north-south) component from NAL, LYR, BAB, and HOR, color coded according to the color bar at the right, in the range from 0 to 1.0 Hz. A wave burst with frequency between 0.2 and 0.5 Hz appeared at all four stations between 0945 and 0953 UT with similar amplitude, but was slightly more intense at LYR. This wave burst is evidence of ion cyclotron waves from the magnetosphere following field lines down to the ionosphere somewhere near Svalbard. The waves occurred during a geomagnetically quiet interval: $Kp = 0+$, 1 and $Dst = 0$, 1 nT.

[12] The wave burst also appeared, with much lower amplitude, in data from a similar search coil instrument located at Sondrestromfjord, Greenland, some ~6 h magnetic local time westward of Svalbard, but also at near-cusp latitudes. No evidence of the wave burst was recorded by search coil instruments at Iqaluit, Canada or South Pole Station, Antarctica, two near-cusp latitudes sites ~1 h MLT
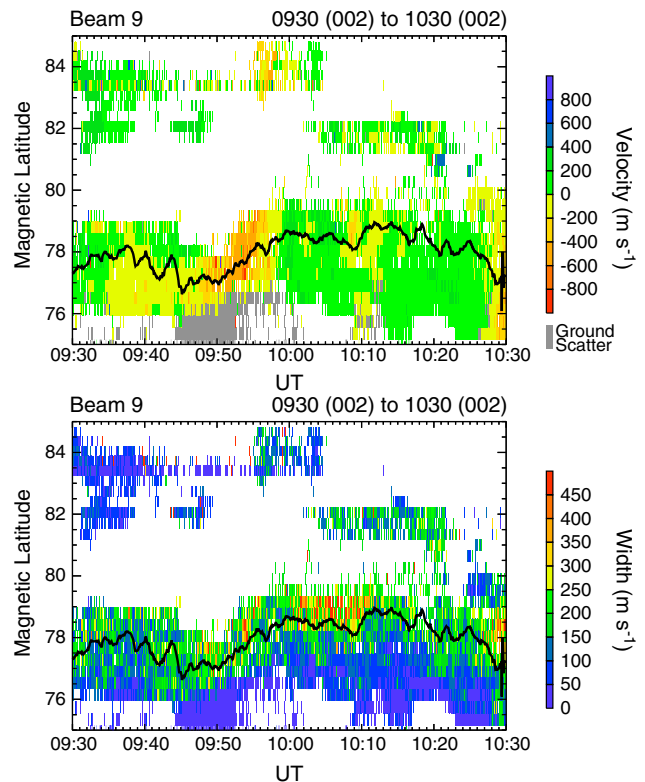
Figure 5. High time resolution beam 9 Hankasalmi SuperDARN radar returns from 0930 to 1030 UT. (top) Flow away from the radar (orange-red, northward) extends across several beams near or shortly after the time of the wave burst near 0950 UT. (bottom) The boundary of increased spectral width (the 220 m s^{-1} boundary is marked on both panels with a black line), usually associated with the open/closed field line boundary, is clear throughout the interval. The strong flow is embedded in this boundary region.
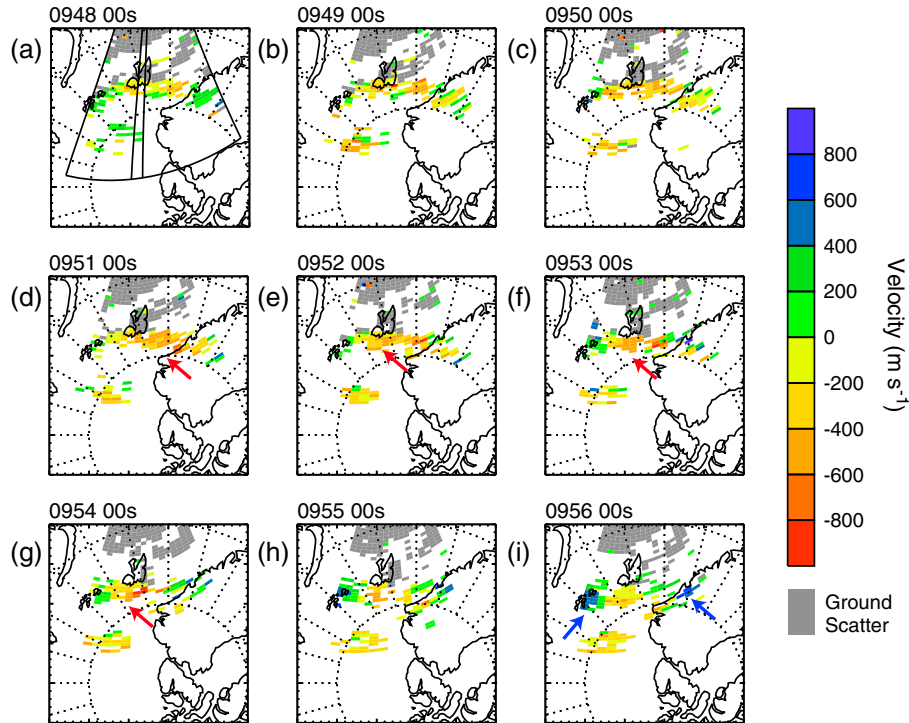
Figure 6. A sequence of Hankasalmi SuperDARN radar velocity map plots in magnetic latitude-magnetic local time coordinates (as used in Figure 1) from 0948 to 0956 UT. Flow away from the radar (orange-red, northward) can be seen to propagate azimuthally eastward across the Hankasalmi field of view.

farther west. Table 2 shows the maximum peak-to-peak amplitude of the wave burst, near 0952 UT, as recorded at each of these stations. The wave burst also appeared in search coil data from most stations in the Finnish pulsation magnetometer array (from Kilpisjärvi, $L = 5.9$, to Oulu, $L = 4.4$, but not at Nurmijärvi, $L = 3.3$). Because data from these stations is provided without calibration, we show in Table 2 the signal-to-noise ratios of the four Svalbard stations along with those from several of the stations in the Finnish array.

[13] Figure 3 shows 10 s cadence geomagnetic component data from a chain of stations in the IMAGE magnetometer network including all those at Svalbard (Table 3), arranged in order of decreasing magnetic latitude roughly along the magnetic meridian, for the time interval from 0900 to 1100 UT 2 January 2011. During this interval a recurrent series of irregular Pc 5 or TCV-like signals appeared. Since the 1970s such activity has been the focus of several publications (e.g., references in *Kurazkovskaya and Klain* [2000]), in which these signals are denoted IPCL (irregular pulsations, continuous, long), and are described as characteristic of the polar cap and dayside cusp regions. Similarly, *Urban et al.* [2011] noted that two frequency bands were prominent near the open-closed boundary: the Pc 5 band, and a band with periods greater than 10 min, which they called long-period modes.

[14] *McHenry et al.* [1990] noted that many such quasi-continuous dayside high-latitude magnetic pulsations might be considered to be caused by steady, traveling ionospheric convection vortices. Indeed, it is often difficult to distinguish TCVs from irregular Pc 5 pulsations (IPCL) in a given time series. *McHenry et al.* [1990] found that the clearest traveling vortex events were associated with low solar wind speed,

which they attributed to an event selection effect, but also noted that the largest pulsations tended to occur at these latitudes when the solar wind velocity was high. Early studies suggested the source of these pulsations was in changes of the interplanetary magnetic field (IMF), including sporadic reconnection [*Bolshakova and Troitskaya*, 1982], but *Kurazkovskaya and Klain* [2000] found evidence that many bursts of IPCL occurred during times when no IMF reorientations occurred; they instead suggested that this activity could be a manifestation of the intermittency of a turbulent SW flow, and were related to stochastic current structures in the polar cusp. More recent studies of TCVs have shown the majority of them to be generated in interactions between the solar wind/IMF and Earth's bow shock [*Murr and Hughes*, 2003; *Kataoka et al.*, 2003], which are enhanced when the IMF is oriented radially (with largest component toward or away from the Earth-Sun direction). This corresponds to IMF cone angles near 0° or 180°.

[15] Figure 4 combines observations from search coil and fluxgate magnetometers on Svalbard. The upper trace in Figure 4 shows the north-south (X) component of the Longyearbyen search coil data, bandpass filtered in the range from 0.1 to 0.5 Hz. The remaining traces in Figure 4 show the magnetic equivalent convection obtained from the same IMAGE magnetometers as in Figure 3, in the format originally presented by *Friis-Christensen et al.* [1988] and *Glassmeier et al.* [1989]: the magnetic disturbance vectors, in local magnetic coordinates, are rotated 90° counterclockwise and displayed in increments of 10 s. Two features distinguish the 0945–1005 UT pulse in the IMAGE data: First, clear rotations near 0930, 0945–1005, and near 1025 UT appear at all stations poleward of 71°
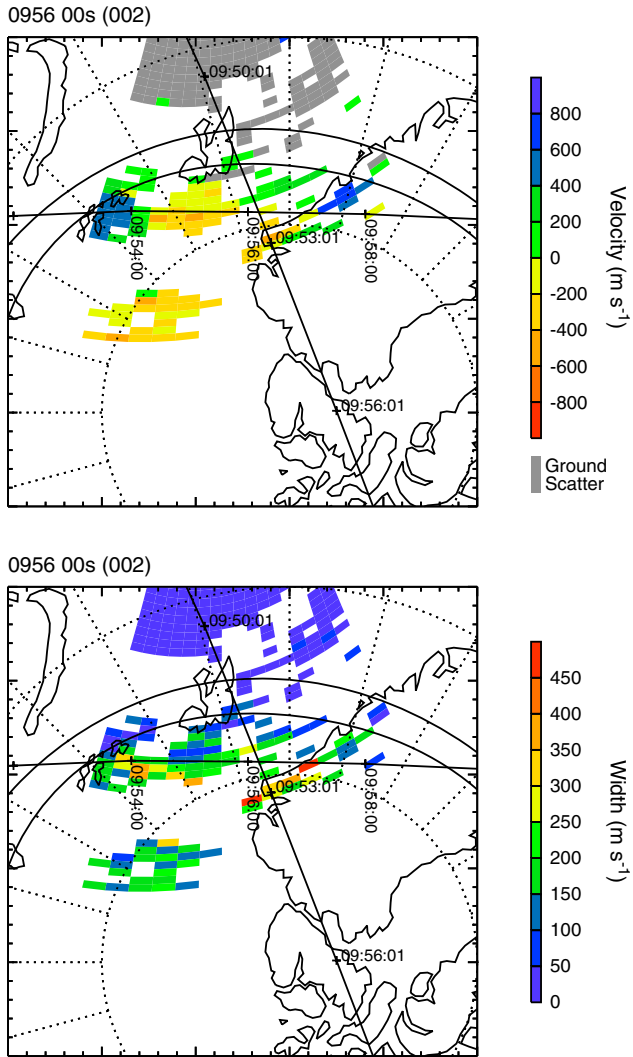
Figure 7. Magnetic latitude-magnetic local time projection (as used in Figure 1) of the (a) velocity and (b) spectral width data from the Hankasalmi SuperDARN radar at 0956 UT. Also shown in both panels are the footprints of the DMSP F17 and NOAA 19 overpasses and a typical auroral oval, as shown in Figure 1.

magnetic latitude, but a significant perturbation only appears at the mainland stations from 0950 to 1005 UT. Second, an EMIC wave burst appeared at the beginning of this pulse, but no such wave burst appeared during the other pulses. However, detailed analysis of the magnetic equivalent convection based on this same data set suggests that two other pulses of those shown in Figure 3, near 0930 and 1025 UT, might also be TCVs. Data from Cluster (to be shown in section 5) provide additional evidence consistent with this suggestion.

[16] The similarity of the vortical patterns at all five higher-latitude stations and the weaker signatures at lower latitudes suggests that the center of the vortical motions was near to (or possibly poleward of) Svalbard. Because of the close longitudinal spacing of the Svalbard stations, however, we cannot confidently infer in what direction the vortex was travelling from the magnetometer data alone.

3. SuperDARN Hankasalmi Radar and DMSP Satellite Data

[17] SuperDARN [*Greenwald et al.*, 1995; *Chisham et al.*, 2007] data during the interval under investigation are provided by the Hankasalmi radar in Finland. Hankasalmi is a Stereo SuperDARN radar [*Lester et al.*, 2004], sounding two radar channels simultaneously. Here channel A of the radar employed a full 16-beam scan of 45 km range gates, starting at a range of 180 km. Channel B was restricted to a single beam, beam 9, pointing northward again with 45 km range gates. The integration time of the radar was 3 s, yielding a full radar scan from Channel A every minute, and single beam data with 3 s time resolution on Channel B. The range-finding algorithm used here includes the corrections for 1½-hop ionospheric backscatter as discussed by *Yeoman et al.* [2001], *Chisham et al.* [2008], and *Yeoman et al.* [2008].

[18] Figure 5 shows the Hankasalmi Channel B high time resolution beam 9 radar returns from 0930 to 1030 UT. The location of the Hankasalmi field-of-view, with beam 9 highlighted, is shown in Figure 6a. In Figure 5 the upper panel presents Doppler velocity, and shows flow away from the radar (orange-red, poleward) during the time of the wave burst near 0950 UT. Although not shown in Figure 5, poleward flows extended in azimuth across several beams during this time interval, and the onset of poleward flow showed a clear eastward propagation of the flow signature. The lower panel of Figure 5 shows the spectral width: the equatorward boundary of the region of increased spectral width, usually associated with the open/closed field line boundary [*Baker et al.*, 1995; *Moen et al.*, 2000; *Villain et al.*, 2002; *Chisham and Freeman*, 2003] is clear throughout the interval, and the spectral width boundary at 220 m s^{-1} is marked with a black line in both panels. The 220 m/s spectral width boundary has been frequently used in the literature as a proxy for the dayside polar cap boundary [see, e.g., *Moen et al.*, 2000; *Oksavik et al.*, 2004]. The strong poleward flow is embedded in this spectral width boundary region.

[19] Figure 6 shows a sequence of SuperDARN velocity data from Channel A as map plots in magnetic latitude-magnetic local time coordinates, from 0948 to 0956 UT. The flow at first is low and predominantly toward the radar. Later, flows directed away from the radar develop in the central beams, whereas flow toward the radar persists in the outer beams (see the blue arrows in Figure 6i). The region of strong flow away from the radar (colored red in the figure) can be seen to move azimuthally in an eastward (antisunward) direction, but to remain at a constant latitude (see the red arrows in Figures 6d–6g). Such flows are consistent with what is expected from a twin vortex flow— thus providing strong evidence that this event is indeed a traveling convection vortex.

[20] As shown in Figure 1, the DMSP F17 spacecraft passed westward to the north of Svalbard from 0954 to 0958 UT, just after the EMIC wave burst, while the NOAA 19 spacecraft passed through the same region in a south-north direction. Figure 7 shows the footprints of these spacecraft overpasses superposed on a magnetic latitude-magnetic local time projection of the Hankasalmi radar velocity and spectral width data at 0956 UT. Both spacecraft passed through the region of enhanced flow and high spectral width
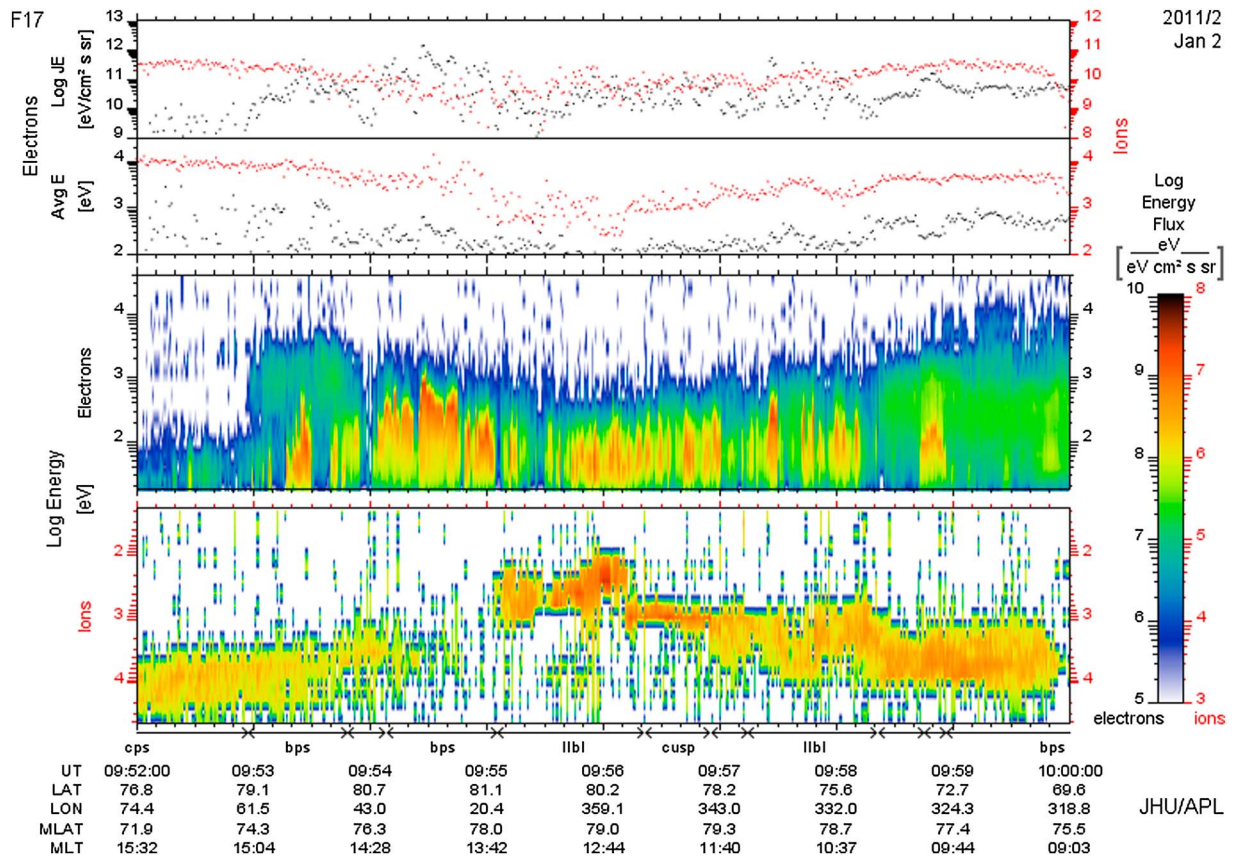
Figure 8. Plot of DMSP F17 precipitating electron and ion data from 0950 to 1002 UT 2 January 2011.

seen by the radar. Figure 8 shows precipitating electron and ion data obtained by DMSP F17 from 0952 to 1000 UT on this day. Magnetospheric regions identified using the JHU/APL online spectrogram viewer (http://sd-www.jhuapl.edu/Aurora/spectrogram/index.html) are shown at the bottom of the figure. The spacecraft was identified as being in the low-latitude boundary layer (LLBL) from 0955:05 to 0956:52, in the cusp from 0956:22 to 0956:56, and again in the LLBL from 0956:56 to 0958:22 UT. These boundaries will be compared to satellite data from NOAA 19 in section 5.

4. Observations in the Western Greenland Sector

[21] Near 0955, at approximately the same time the strongest TCV appeared over Svalbard, a TCV appeared at several stations in the Western Greenland magnetometer chain. Figure 9 shows the magnetic equivalent convection, in the same format as Figure 4, obtained using the Western Greenland stations listed in Table 3, ranging in magnetic latitude from 67.1° to 84.57°. A clear rotation was again evident from 0945 to 1005 UT, with peak convection centered near 75°–77° MLAT but dropping off only gradually poleward and equatorward. A weaker vortex was again observed near 0930 UT, but very little activity was evident after 1005 UT. Stokkseyri SuperDARN radar Doppler velocity data (not shown) revealed a region with transient velocity in this same part of Western Greenland, consistent with the magnetometer data within its field of view. These Greenland observations provide evidence that during this

event convection vortices were set up on both sides of local noon, consistent with the "canonical" TCV event presented by *Lühr and Blawert* [1994].

[22] As was noted above, the only available search coil magnetometers in this region, at Sondrestromfjord and Iqaluit, were both at somewhat lower magnetic latitudes. Only Sondrestromfjord showed any evidence of a Pc 1 burst, and that was very weak. The absence of Pc 1 activity at these
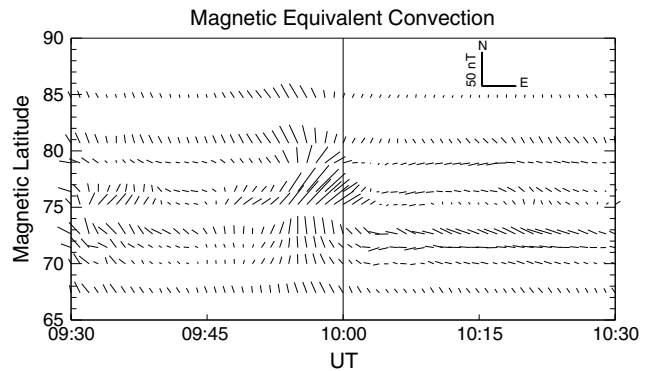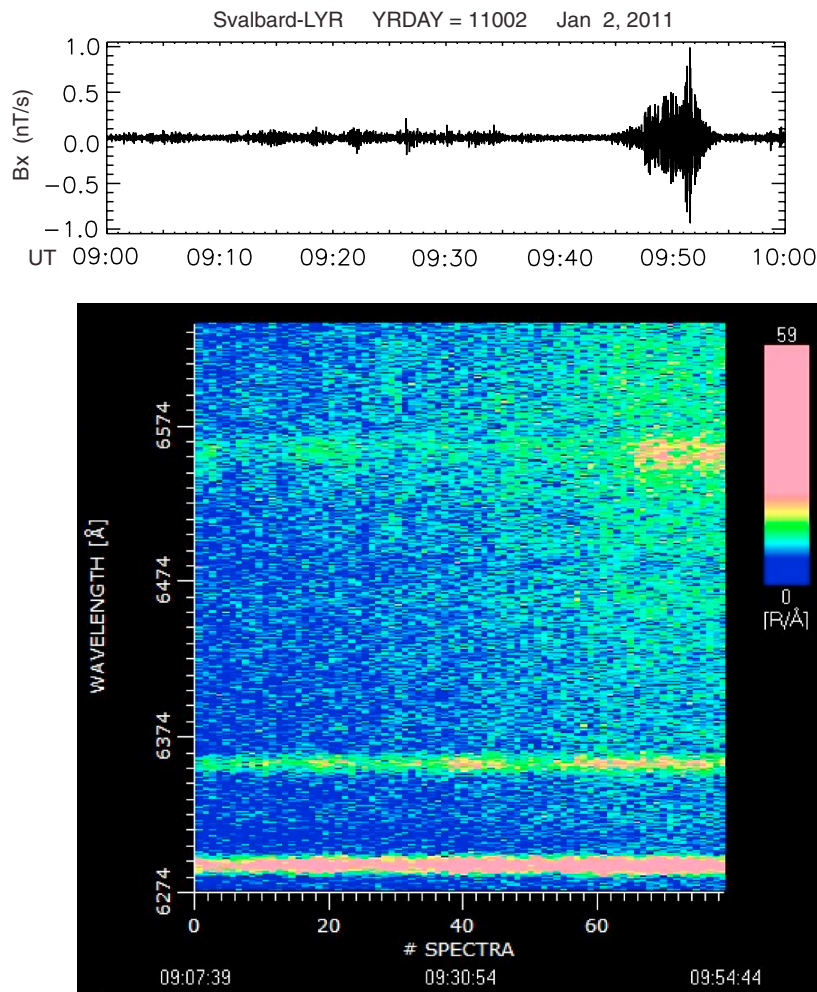

Figure 9. Plot of the magnetic equivalent convection as a time series of vectors from 0930 to 1030 UT 2 January 2011, based on 1 min geomagnetic component data from the western Greenland magnetometer array listed in Table 3, arranged in order of decreasing magnetic latitude.

Figure 10. A line plot of the north-south (*X*) component of Longyearbyen search coil magnetometer data, bandpass filtered in the range from 0.1 to 0.5 Hz, from 0900 to 1000 UT 2 January 2011 (top), and part of the spectrum obtained simultaneously by the "Half Meter White" Ebert-Fastie optical spectrometer located at the Kjell Henriksen Observatory, Longyearbyen. Spectra were obtained with a 35 s cadence.

stations is not surprising, however, both because of their somewhat lower latitude, and because of their local time, roughly 4.5 h before local noon. A statistical study of TCV / Pc 1 burst events by *Posch et al*. [2011, also manuscript in preparation, 2013] found that although TCV events could be identified in ground magnetometer data up to 6 h before local noon, Pc 1 bursts associated with these TCV events were only observed within 3 h of local noon.

5. Observations of Precipitating Energetic Particles

[23] This is not the first time that proton precipitation has been observed in association with a TCV-like event. *Ebihara et al*. [2010] presented observations of localized (spot-like) auroral hydrogen emissions at 486.1 nm (the H_β line) with durations of ~1–2 min at South Pole Station, Antarctica, in conjunction with two magnetic impulse events (MIEs). They interpreted these emissions as resulting entirely from precipitating protons, but found no clear correspondence between the spots and wave power in the Pc 1 range observed on the ground. During the first of the two cases shown, there was no clear enhancement in Pc1 power (as could be detected by the University of New Hampshire/ Augsburg College search coil magnetometer at South Pole) associated with either the MIE or the short-lived proton emission. In the second case shown, the search coil magnetometer detected moderately strong, bursty broadband Pi1 activity for over an hour before, during, and after the MIE; localized auroral hydrogen emissions were observed for ~1.5 min just after the MIE, and no intensification of wave activity accompanied the auroral "spot." As will be shown below, the event reported here is distinguished from those presented by *Ebihara et al*. [2010] in two ways: (a) there was a clear temporal association between the ground-observed proton precipitation and the appearance of EMIC waves, and (b) satellite observations were available to characterize the energy of the precipitating protons.

[24] Figure 10 shows a 1 h segment of bandpass-filtered X-component search coil magnetometer data from Longyearbyen (top panel), and part of the spectrum obtained simultaneously by the Half Meter White Ebert-Fastie optical
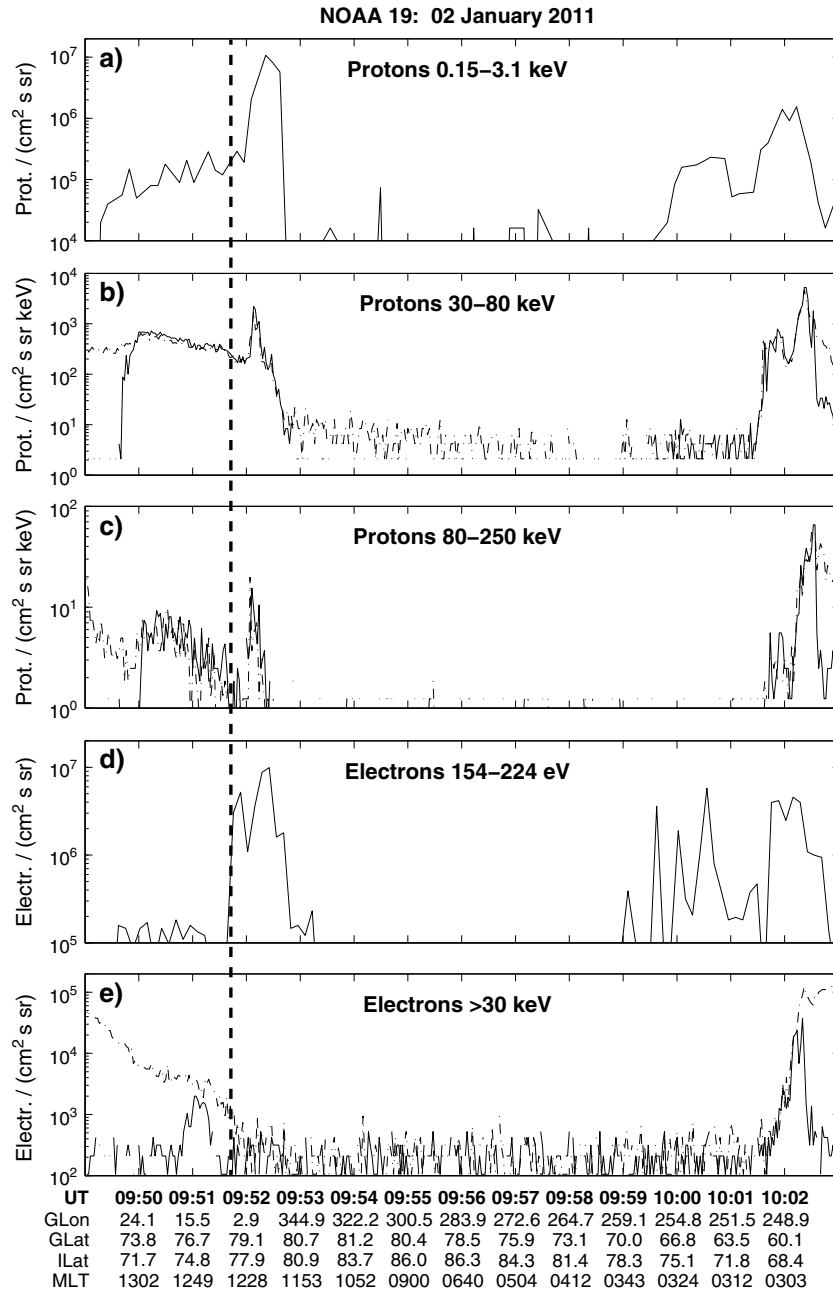
Figure 11. NOAA 19 satellite data during the Pc1 burst on 2 January 2011. The solid traces show data from the 0° (zenith-pointing) detectors, which measure particles near 0° pitch angles, and the dashed lines from the 90° MEPED detectors, which measure particles near 90° pitch angles. The vertical dashed line indicates the open-closed boundary, determined as described in the text.

spectrometer at the Kjell Henriksen Observatory in Longyearbyen, which has an angular field of view of 1 degree, and is pointed upward along the local magnetic field line (pointing to the magnetic zenith). Spectra were obtained with a 35 s cadence. In contrast to the steady and forbidden atomic oxygen (OI) lines at 630.0 and 636.4 nm, a weak, relatively broad signal in the H_α line (656.3 nm) brightened suddenly at 0947 UT, approximately the time of the intensification of the Pc 1 wave burst, and continued with some variability in amplitude before the instrument was automatically turned off at 0954 UT to prevent contamination/overexposure by sunlight.

[25] In situ evidence of precipitating protons was also available during this event. The NOAA 19 spacecraft [*Evans and Greer*, 2000], in a polar orbit at ~815 km altitude, passed over the archipelago of Svalbard between 0951 and 0952 UT, during the Pc1 burst (Figure 1). Figure 11 shows evidence of precipitating protons and electrons characteristic of both closed field lines and of open field lines.

[26] Large fluxes of trapped protons in the 30–80 and 80–250 keV channels (Figures 11b and 11c) appeared from 0947 (not shown) to shortly before 0953 UT. Precipitating fluxes of 30–80 keV protons (Figure 11b) reached the same level as the trapped protons from 0949:40 to

NYA ASI : 630.0 nm : JANUARY 2, 2011
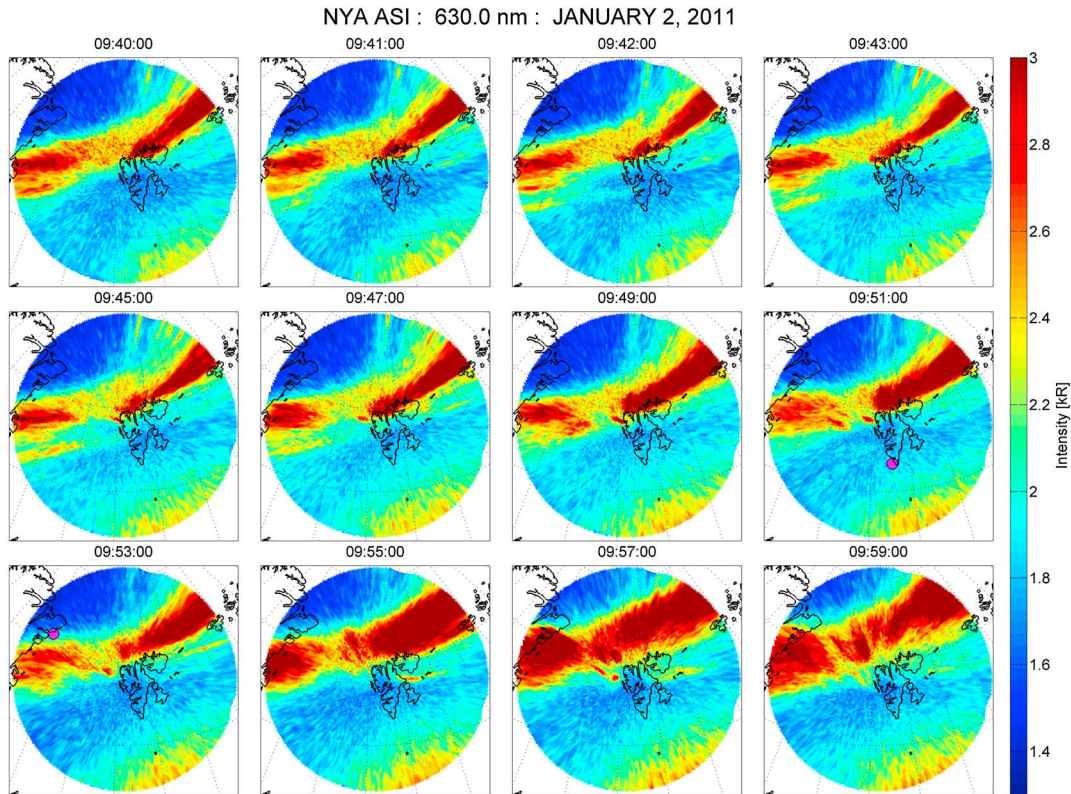
Figure 12. (a) A sequence of 630.0 nm (OI) all-sky images projected to a geographic frame of reference at an altitude of 250 km, produced from observations by the University of Oslo auroral imager at Ny-Ålesund, from 0940 to 0959 UT, 2 January 2011. The rose-colored dot marks the NOAA satellite pass when it was inside the image frame. Emission intensities are scaled according to the color bar at right. (b) A sequence of 557.7 nm (OI) all-sky images projected to a geographic frame of reference at an altitude of 150 km, produced from observations by the University of Oslo auroral imager at Ny-Ålesund, from 0940 to 0959 UT, 2 January 2011. The rose-colored dot marks the NOAA satellite pass when it was inside the image frame. Emission intensities are scaled according to the color bar at right. (c) Keograms of auroral emission intensity at 630.0 nm wavelength (top) and 557.7 nm (bottom) produced from observations by the University of Oslo auroral imager at Ny-Ålesund, from 0930 to 10:00 UT, 2 January 2011. Emission intensities, scaled according to the color bars at right, are shown as a function of north-south zenith angle (vertical axis) and universal time (horizontal axis).

0952:40 UT, at which time the 30–80 keV proton fluxes dropped to background levels. Similarly, precipitating fluxes of 80–250 keV protons (Figure 11c) reached the same levels as the trapped protons from 0950 to 0952:20 UT. The fact that the pitch angle distribution within and near the loss-cone was isotropic indicates strong pitch angle scattering, consistent with strong wave-particle interactions, but does not imply that the flux was isotropic over the whole pitch angle distribution, i.e., outside the loss cone [*Sergeev et al.*, 1983]. Comparison to Figure 1 indicates that the region of isotropic fluxes included the flux tubes over Svalbard, so it is consistent with the ground-based optical data shown in Figure 10 and with the inferred location of the Pc 1 wave burst on field lines overhead of Svalbard.

[27] NOAA 19 data can also be used to determine the location of the open/closed polar cap boundary, shown in Figure 11 by a vertical dashed line. NOAA-19 crossed the 30 keV electron trapping boundary at 09:51:49 UT (78.62 GLAT, 5.83 GLON, 77.32 MLAT, 12:33 MLT). On the equatorward side of this boundary the particle population was composed of energetic (>30 keV)

electrons of magnetospheric origin; i.e., on closed field lines. On the poleward side enhanced fluxes of 154–224 eV magnetosheath electrons that are characteristic of open field lines appeared (09:51:47–09:52:43 UT, 78.55–80.32 GLAT, 6.30–350.89 GLON, 77.22–80.05 MLAT, 12:33–12:06 MLT). Consequently, for this event the 30 keV electron trapping boundary appears to be a reasonable proxy for the open-closed field line boundary [*Moen et al.*, 1996, 1998; *Oksavik et al.*, 2000].

[28] In addition, just poleward of the open-closed boundary, on newly opened field lines, there were significant enhancements in the proton data. A spike of high-energy protons (30–80 keV and 80–250 keV) was seen at 09:52:09 UT (79.33 GLAT, 0.84 GLON, 78.35 MLAT, 12:24 MLT). Enhanced fluxes of low-energy protons of magnetosheath origin (Figure 11a) were also seen at 09:52:07–09:52:39 UT (79.26–80.22 GLAT, 1.36–352.15 GLON, 78.25–79.85 MLAT, 12:25–12:08 MLT). *Moen et al.* [1996] and *Lockwood and Moen* [1996] have reported enhanced ion populations on newly opened field lines and related it to transient events and dynamics in the LLBL. It
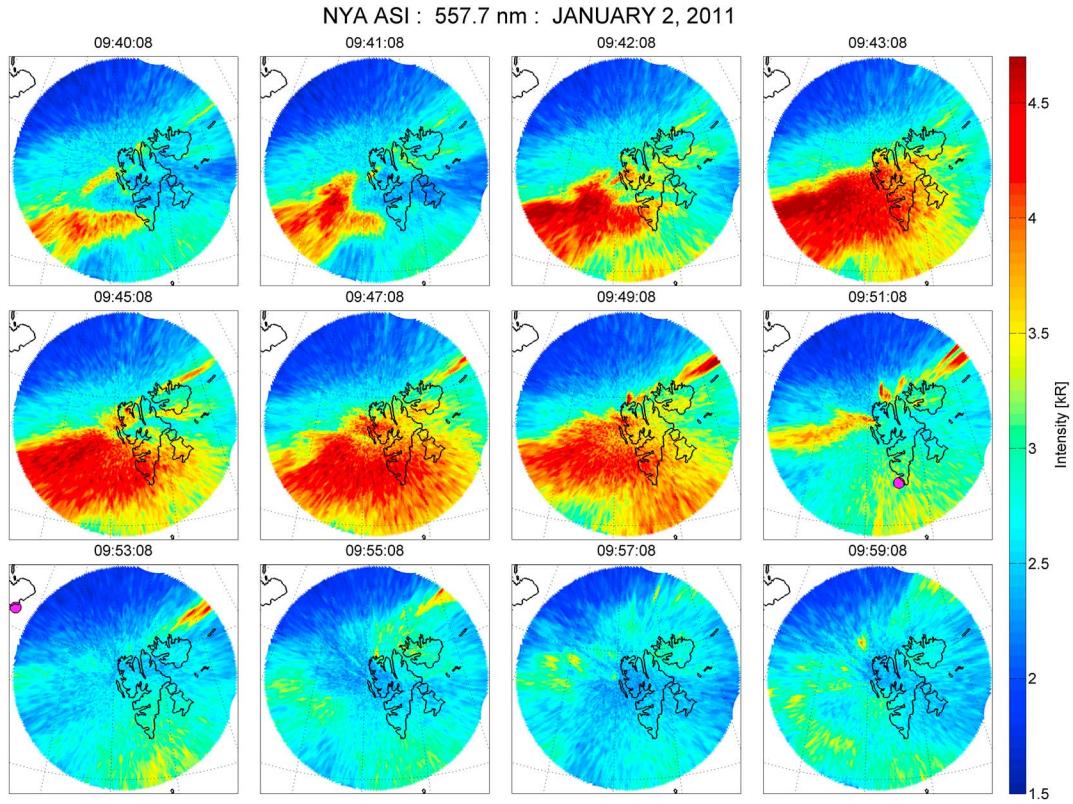
NYA ASI : 557.7 nm : JANUARY 2, 2011

Figure 12. (continued)

is therefore reasonable to assume that the proton spike was on newly opened field lines, in the outer low-latitude boundary layer. We have no information, however, on whether the energetic component of this proton spike was related to the generation of Pc 1 wave activity.

[29] The ground tracks of DMSP F17 and NOAA 19 in Figure 1 have been color coded and annotated to display the above features in the particle data. The green and blue colors on the horizontal track denote the open and closed regions, respectively, derived from DMSP data. The low-
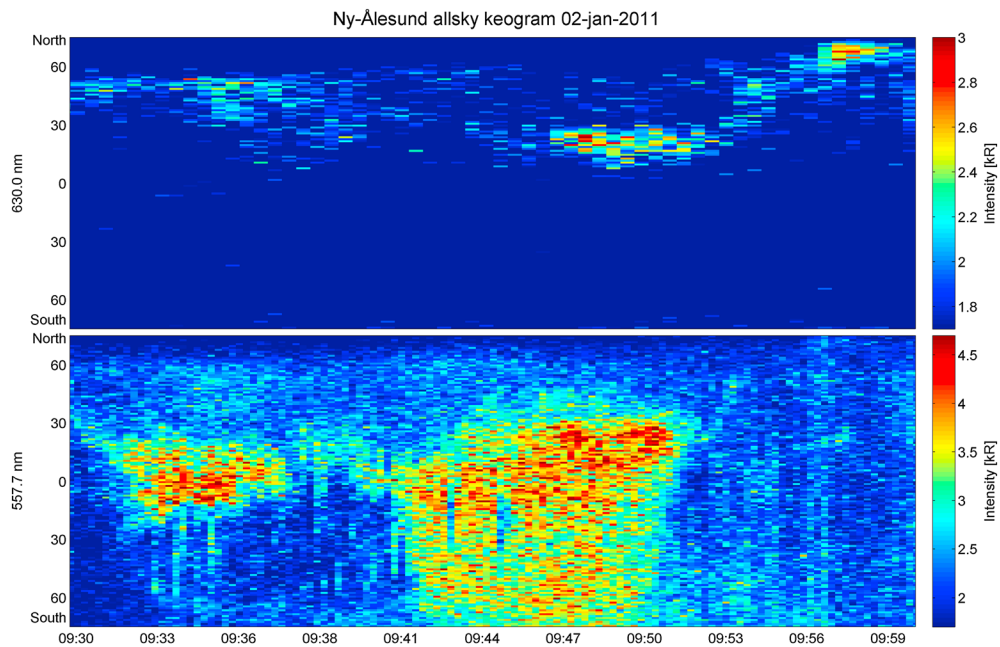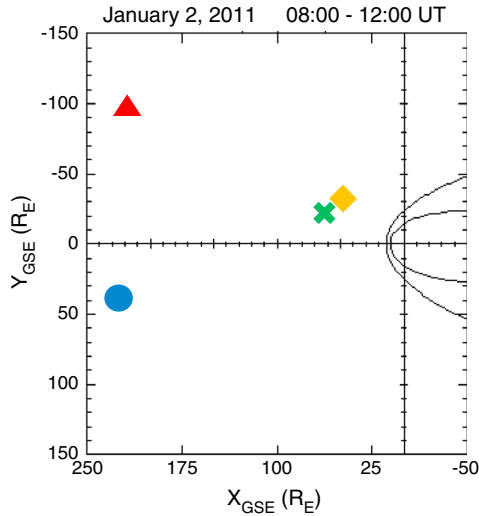

Figure 12. (continued)

Figure 13. Locations of ACE (blue), Wind (red), THEMIS B (green), and THEMIS C (yellow) in the solar wind upstream from Earth's bow shock during the TCV/EMIC wave event of 2 January 2011. Plot adapted from one obtained from http://sscweb.gsfc.nasa.gov.

energy electron spike observed by NOAA 19 is marked on the diagonal track (NOAA 19) with a green line, and the green arrow denotes the 30 keV electron trapping boundary. The low-energy proton spike is marked with a red line, and the red arrow denotes the high-energy proton spike. It can be seen that the boundaries of magnetospheric regions identified by DMSP, NOAA, and SuperDARN are consistent with each other, even given the ~3 min time delay between the passage of NOAA 19 and DMSP, supporting the interpretation that the EMIC wave signature was on closed field lines.

[30] Auroral images during the time of this event were obtained by the University of Oslo all-sky imager at Ny-Ålesund, an intensified CCD camera fitted with a filter wheel operating at wavelengths of 630.0 nm (red) and 557.7 nm (green). These auroral emissions stem from precipitating electrons exciting ambient neutral atomic oxygen (OI) to the 1S and 1D metastable states, respectively. The all-sky images have been projected onto a geographic frame of reference assuming peak emission altitudes for the 630.0 and 557.7 nm emissions to be 250 and 150 km, respectively. Because of the lack of a priori knowledge of the energy distribution of the auroral particles, these assumed altitudes are subject to uncertainties [*Moen et al.*, 2000]. However, this is not at all critical for the current study.

[31] Figures 12a and 12b display a sequence of 12 images of 630.0 (red) and 557.7 nm (green) wavelength, respectively, from 0940 to 0959 UT. We draw the reader's attention to two different categories of auroral forms. The red line aurora was located in the northern part of the field of view in Figure 12a, and the green line aurora, or diffuse aurora, was located in the southern part of the field of view in Figure 12b. While this diffuse aurora occurred exclusively in the green channel, the red line auroral forms poleward of it could also appear in the green channel. These two subclasses of daytime auroral activities have previously been associated with different magnetospheric source regions. *Lorentzen et al.* [1996], *Moen et al.* [1998], and *Lorentzen*

and Moen [2000] associated the diffuse 557.7 nm aurora with the central plasma sheet source located on closed field lines. *Sandholt et al.* [1998] referred to this class as Type 3 aurora. The red-green auroral forms on the poleward side were associated with cusp auroral emissions on open field lines by *Moen et al.* [1998] and *Lorentzen and Moen* [2000]. Under northward IMF Bz conditions (with IMF clock angles < 45°), as was the case during this event (cf. Figure 16), these would be cusp aurora of Type 2 (lobe reconnection) in the *Sandholt et al.* [1998] classification. Notably, these red line auroral intensifications were filamentary and their intensity increased with distance from the center pixel (i.e., with increasing range from the optical site). This indicates auroral rays for which geographic projection does not work accurately [*Moen et al.*, 1995].

[32] The auroral activity presented in Figure 12b bears strong resemblance to the shock aurora presented by *Lorentzen and Moen* [2000] and *Zhou et al.* [2009], where the diffuse aurora filled in a broad latitude region equatorward of the cusp aurora. *Zhou et al.* [2009] also addressed the rayed cusp auroral signatures of Alfvénic aurora, suggesting that they were stimulated by kinetic Alfvén waves launched by magnetic reconnection [*Stasiewicz et al.*, 2001; *Chaston et al.*, 2005].

[33] Spatially, the cusp auroral precipitation (at 630.0 nm, Figure 12a) appeared with greatest intensity in the eastern half of the all-sky field of view. Temporally, there was an intensification of cusp aurora starting at 0945 UT and remaining at nearly constant latitude until 0953 UT. After this time it remained intense but retreated poleward.

[34] In contrast, the 557.7 nm diffuse aurora (Figure 12b) surged into the field of view from the west; it appeared overhead of Svalbard around 0942 UT and expanded eastward and equatorward until it attained maximum coverage of the field of view at 0947 UT; after this time it retreated back again eastward and poleward until it almost disappeared at 0951 UT. Later images in Figure 12b show that beyond 0951 UT there were still some patchy diffuse 557.7 nm auroras, but they were much weaker.

[35] Figure 12c, a keogram produced from the entire set of all-sky images at both wavelengths, shows the difference in occurrence time between these two types of aurorae. The time interval when diffuse aurora appeared overhead, from 0942 to 0951 UT, was ~2 min earlier than the Pc 1 wave burst (0945–0953 UT). The diffuse aurora is caused by electrons scattered into the loss cone [*Zhou et al.*, 2009] that can immediately access the ionosphere, while Alfvén waves take ~2 min longer to arrive. This provides a physical explanation for the time delay between the occurrence of diffuse 557.7 nm auroral emissions and the Pc 1 burst.

[36] Both Figures 12c and 12a show that the higher-latitude Alfvénic cusp auroral intensification lasted from 0946 to 0953 UT, matching the duration of the Pc 1 wave burst. We interpret this temporal match to be accidental, and not indicative of a close physical coupling, for three reasons. First, the proton aurora were observed overhead of Longyearbyen, at a latitude associated with the diffuse aurora. Second, as *Zhou et al.* [2009] noted, both electrons and protons can be pitch angle scattered by a compression of the outer dayside magnetosphere. The fact that the Pc 1 wave packet observed at Longyearbyen was temporally aligned with the overhead proton aurora, as shown in

January 2, 2011   08:00 - 12:00 UT
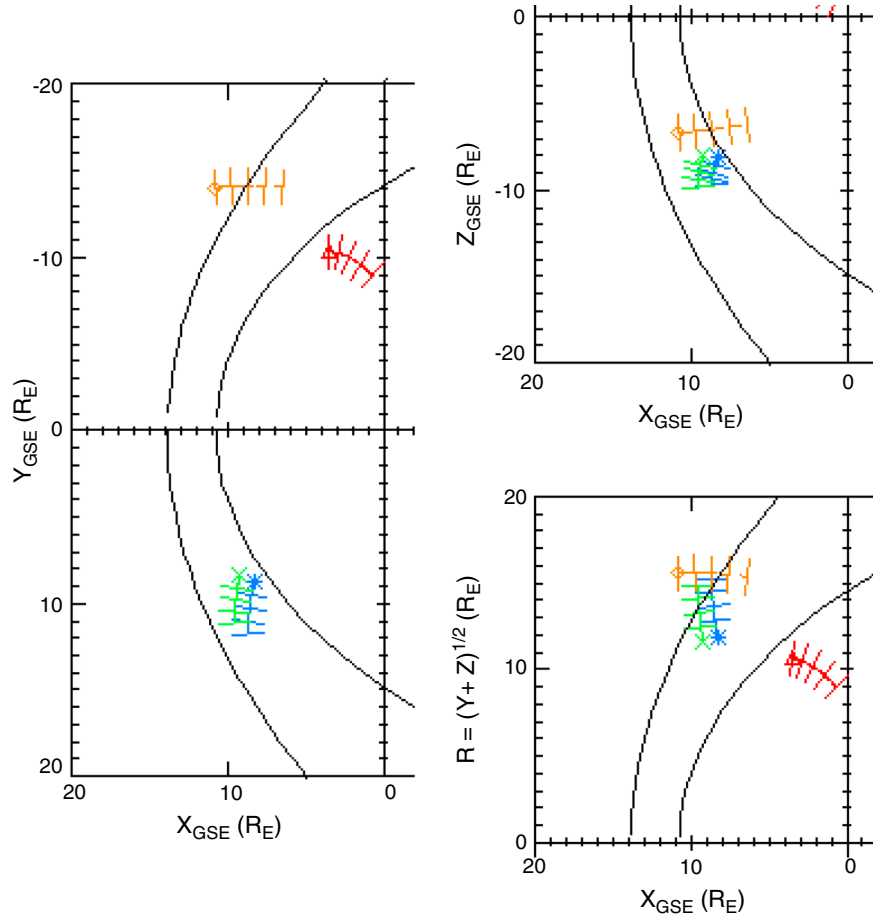
Figure 14.   Locations of Geotail (orange), Cluster 2 (blue), Cluster 4 (green), and THEMIS-A (red) from 0800 to 1200 UT on 2 January 2011. The symbol for each spacecraft trajectory shows its position at 1200 UT. Plot adapted from one obtained from http://sscweb.gsfc.nasa.gov.

Figure 10, is thus consistent with the lower velocity, and hence longer travel time, of precipitating protons than electrons. Such a delay between electron and proton arrival after a transient magnetospheric compression was also evident in the keogram in Figure 1 of *Ebihara et al.* [2010], which showed two bursts of proton aurora observed over South Pole Station, Antarctica, delayed ~2 min relative to two bursts of 557.7 nm emissions. Third, as will be discussed below, the cusp auroral intensification can instead be evidence that lobe reconnection occurred in association with the large transient deflection in the IMF immediately upstream of the bow shock detected by Geotail and Cluster-4 (shown in Figure 16), which greatly increased the already positive IMF Bz component. As noted above, the open-closed boundary coincided with the lower-energy proton and electron signatures in the NOAA data.
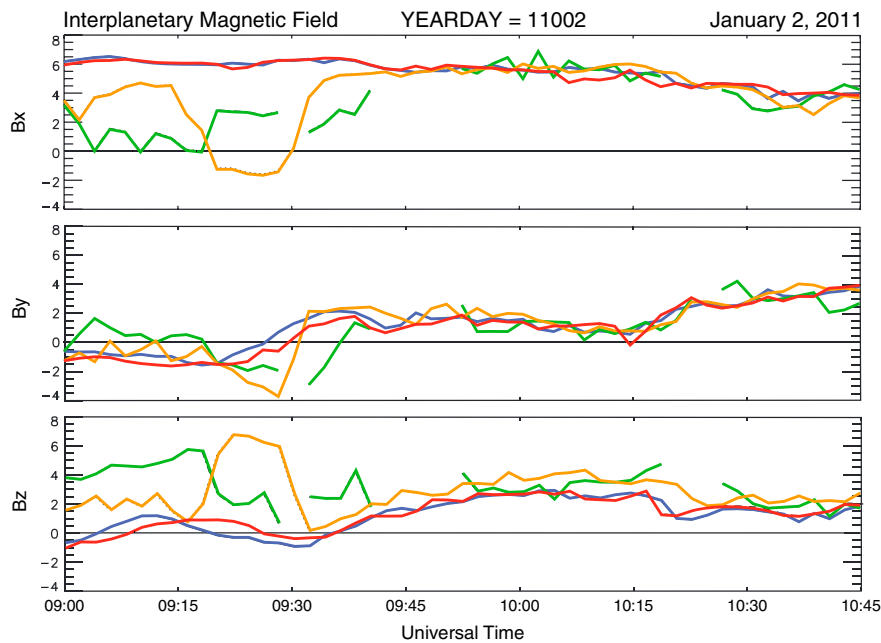
6.   Solar Wind and Interplanetary Magnetic Field Observations

[37] Several spacecraft were in the upstream solar wind during this wave event. Figure 13 shows the positions of ACE (230 R_E upstream), Wind (220 R_E upstream), THEMIS

B (60 R_E upstream), and THEMIS C (50 R_E upstream), in the GSE XY plane, and Figure 14 shows the positions of three spacecraft (Geotail, Cluster 2, and Cluster 4) in the near upstream region relative to nominal bow shock and magnetopause positions, and the position of THEMIS A in the outer dayside magnetosphere. The left-hand panel of Figure 14 shows their positions in the GSE XY plane, as in Figure 13. Geotail moved outward across the dawnside bow shock into the solar wind, and Cluster 2 and 4 moved inward from the solar wind toward the duskside bow shock. The upper right-hand panel shows the positions of Geotail, Cluster 2, and Cluster 4 in the GSE XZ plane; all three were in the Southern Hemisphere. The lower right-hand panel shows the positions of all four satellites in GSE XR coordinates, where R is the distance from the Earth-Sun line. It more clearly shows the locations of the spacecraft relative to the nominal bow shock and magnetopause. At 0950 UT Geotail was near 0725 MLT at 17.7 R_E, and Cluster-4 was near 1630 MLT at 16.8 R_E. The trajectories of Cluster 1 and 3 (not shown) would appear nearly identical to that of Cluster 4 at the scale of these figures, while Cluster 2 passed ~0.9 R_E earthward of the other three, and was inside the magnetosheath during much of this interval. The fourth
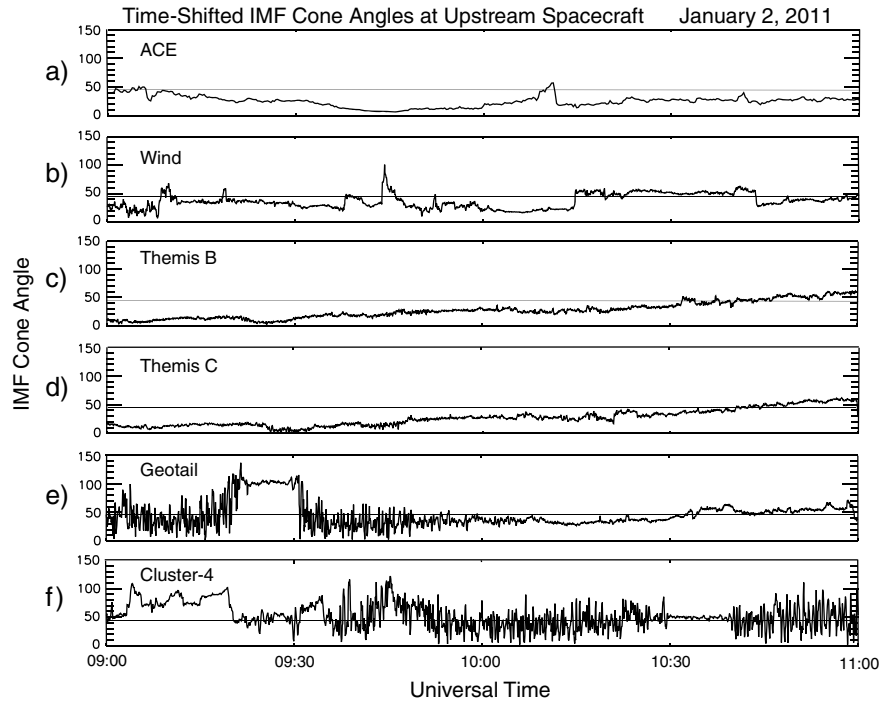
Figure 15. IMF cone angles observed by several upstream spacecraft: (a) ACE, (b) Wind, (c) THEMIS B, and (d) THEMIS C, respectively, each time-shifted to Earth's magnetopause using a solar wind speed of 340 km/s. (e and f) The IMF cone angle measured by Geotail and Cluster-4, respectively, with no time shift. The thin horizontal line in each panel is at 45°.

Figure 16. Superposed plots of the interplanetary magnetic field in GSE coordinates observed by THEMIS B (blue), THEMIS C (red), Geotail (orange), and Cluster 4 (green). The THEMIS B and THEMIS C data have been time shifted by 16 and 13 min, respectively, as described in the text. Cluster 4 data are shown only during times when that spacecraft was upstream of the bow shock.
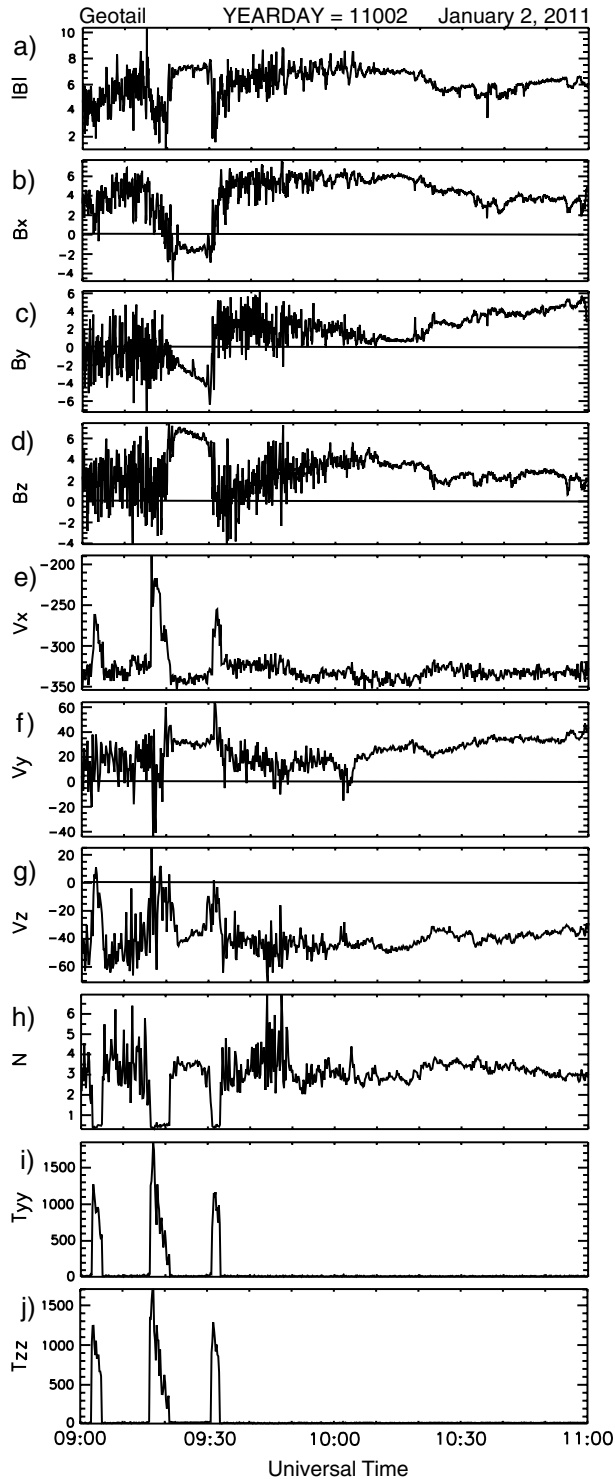
Figure 17. Magnetic field and plasma data from Geotail. (a, b, c, d) Interplanetary magnetic field (in nT): total field and *x*, *y*, and *z* components in the GSE coordinate system, respectively. (e, f, g) Solar wind velocity (in km/s) in the GSE coordinate system, (h) Ion density (in cm^{-3}), and (i, j) perpendicular and parallel ion temperature, respectively (in eV).

spacecraft shown in Figure 14, THEMIS A, was located in the outer dawn sector magnetosphere. The trajectories of THEMIS D and E (not shown) would also appear nearly identical to that of THEMIS A at the scale of these figures.

6.1. Upstream Observations

[38] The spacecraft in the solar wind far upstream of Earth's bow shock on this day observed a steady solar wind and nearly steady IMF orientation both before and during the TCV/Pc 1 burst event. Figures 15a–15d show the IMF cone angle $\theta_{xB} = \cos^{-1}(Bx/B)$ observed at ACE, Wind, THEMIS B, and THEMIS C, respectively, each time-shifted to Earth's magnetopause using the observed solar wind speed of 340 km/s. Each of the four upstream spacecraft observed a predominantly radial IMF ($\theta_{xB} < 45°$) from 0900 to after 1010 UT. This IMF direction is consistent with the dayside magnetosphere being significantly influenced by a quasi-parallel shock and its associated upstream ion foreshock and complex downstream magnetosheath.

[39] Figure 15e shows the cone angle measured by Geotail with no time shift. The excursion of the cone angle to near 100° between ~0920 and 0930 UT is not expected, based on the data from the four upstream spacecraft. This change allowed Geotail to be outside of the ion foreshock, and in the pristine solar wind, during this interval.

[40] Figure 15f shows similar data from Cluster 4, again with no time shift. The cone angle exceeded 45° during several intervals, some of which (as shown in Figure 18 below) were associated with bow shock crossings. Cluster 4 was in the solar wind; however, from 0900 to 0935 UT, and again, consistent with the large cone angles observed by Cluster 4 during this time (which were again unexpected based on the upstream data), no upstream waves were present in any component. Upstream waves were present in all IMF components observed by Cluster 4 (not shown) for most of the remainder of the interval shown in Figure 15, with a clear exception being the interval from ~1030 to 1040 UT. Magnetic field data from Cluster-1 and -3 exhibited similar transitions between relatively quiet and more fluctuating IMF conditions, again associated with changes in the IMF cone angle.

6.2. Observations Near the Bow Shock

[41] Figure 16 shows superposed IMF data in GSE coordinates from THEMIS B, THEMIS C, Geotail, and Cluster-4 from 0900 to 1045 UT. The data are shown as 2 min averages to smooth out the large fluctuations in all three magnetic field components that are characteristic of the ion foreshock (Figure 15). The THEMIS B and THEMIS C data have been time shifted by 16 and 13 min, respectively, to account for the propagation of the solar wind from 60 (50) R_E upstream to the nose of the bow shock, and Cluster 4 data are shown only during times when that spacecraft was upstream of the bow shock. Figure 16 shows that THEMIS B and C observed very similar (but not identical) IMF values throughout this ~2 h interval, and also shows good agreement (within 1 or 2 nT) in all components of the IMF between all four spacecraft after 0940 UT. From 0900 to 0915 UT the *Bx* and *Bz* components of the IMF observed at Geotail were quite different from those observed at THEMIS B and C, and they showed even larger differences between 0915 and 0935 UT. The *Bx* and *Bz* components of
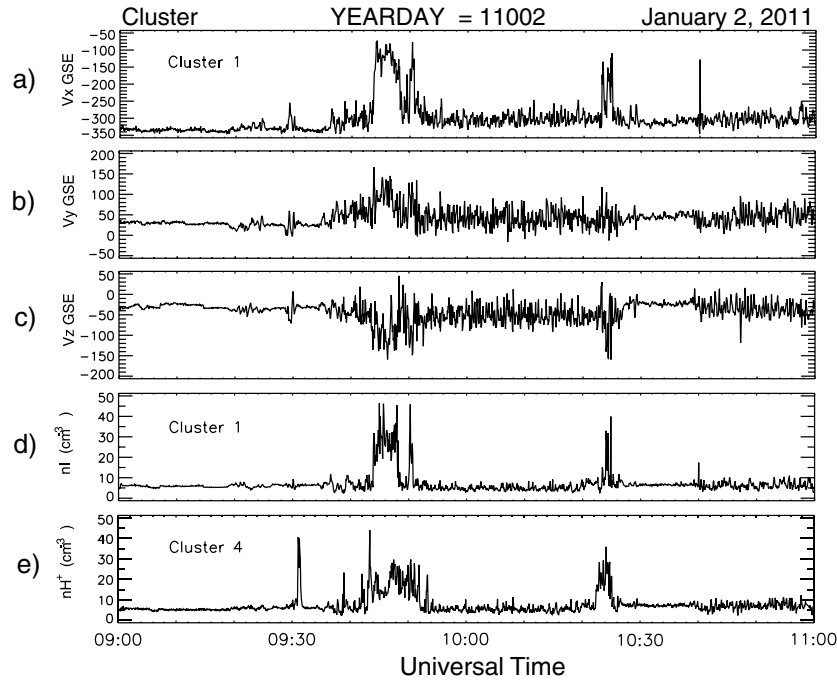
Figure 18. Ion density and solar wind velocity data from the CIS instruments on Cluster. (a, b, and c) Components of the solar wind velocity (in km/s) in the GSE coordinate system measured by the HIA instrument on Cluster-1. (d) Total ion density measured by the HIA instrument on Cluster-1. (e) H + density measured by the CODIF instrument on Cluster-4.

the IMF observed at Cluster 4 between 0900 and 0940 UT also differed greatly from the THEMIS B and C values, and differed substantially from those observed at Geotail as well.

[42] Figure 17 shows vector magnetic field and plasma data from Geotail during this interval. Figures 17a–17d show that all three components of the IMF at Geotail (shown in GSE coordinates) and the field magnitude, exhibited large variability from 0900 to 0920, and again from 0932 (with decreasing amplitude) to ~1005 UT. This indicates that Geotail was in the ion foreshock region during these times, observing upstream waves. There was no upstream wave activity in any component from 0921 to 0931 UT. Figures 17e, 17f, and 17g show that the solar wind speed was near 330 +/− 15 km/s throughout the interval from 0900 to 1100 except for three few-minute intervals of reduced solar wind flow: 0902:45–0905, 0916:30–0921, and 0931–0933 UT. The latter two of these intervals occurred during rotations of the IMF observed at Geotail as it transitioned out of and back into the ion foreshock. The solar wind velocity also exhibited modest rotations, most notable in the Z_{GSE} component, during these three intervals of reduced flow. During these intervals the solar wind ion density (Figure 17 h) dropped precipitously, and the ion temperature (Figures 17i and 17j) rose from ~20 eV to values from ~500 to over 1500 eV for both the ions perpendicular to the IMF direction (Tyy) and parallel to it (Tzz).

[43] Although not as prominent as the sharp drops in ion density and the sharp increases in ion temperature, |B| also showed a noticeable drop during each of these three few-minute intervals (Figure 17a). Each of these intervals thus has several signatures of a hot flow anomaly (HFA), as characterized by *Thomsen et al.*, [1986]: a reduction in |B|,

a reduction in the solar wind speed and a perturbation in direction as if to go around the magnetospheric obstacle, an order of magnitude (or more) increase in ion temperature, and an order of magnitude drop in number density.

[44] These events also have significant differences from typical HFA signatures, however: (1) the reductions in |B| were quite modest; (2) the deflections of Vsw in the Z_{GSE} component were positive, hence toward Sun-Earth line, rather than away from it; and (3) although HFAs are typically associated with discontinuities in the IMF [e.g., as reviewed by *Turner et al.*, 2011], there were no evident IMF discontinuities in the upstream data, as shown in Figures 15 and 16. One would also expect the deflections of Vsw in the Y_{GSE} direction to be negative (away from the Sun-Earth line), but were below noise levels during the first event, strongly negative and then strongly positive during the second event, and strongly positive and then strongly negative during the third event. As will be discussed below, however, a class of spontaneous hot flow anomalies (SHFAs) recently identified by (*Zhang et al.,* submitted manuscript, 2012) and modeled by *Omidi et al.* [2013] develops spontaneously in the ion foreshock region, and is not linked to any IMF discontinuity.

[45] Ion density and bulk velocity data from the CIS instruments on Cluster-1 and Cluster-4 are shown in Figure 18. Although decreases in the ion velocity also appeared at Cluster, they were accompanied by quite different density perturbations than those observed at Geotail.

[46] The three components of the solar wind bulk velocity (in the GSE coordinate system) measured by the CIS-HIA instrument on Cluster 1 are shown in Figures 18a, 18b, and 18c. The X component of the bulk ion velocity was near −330 km/s before 0930, dropped sharply to ~ −100 km/s near

0944 UT, and except for the two brief intervals near 0930 and 1024 UT returned to values near −300 km/s but with much greater variability in all three components.

[47] Figures 18d and 18e show ion density from the CIS-HIA instrument on Cluster-1 and proton density from the CIS-CODIF instrument on Cluster-4, respectively. Number densities near 6 cm^{-3} were observed throughout the 0900–1100 interval at both spacecraft except during three brief periods when the density increased substantially: ~0930, ~0943–0952, and 1022–1025 UT. The times of these brief periods differed only slightly between the two spacecraft. Both instruments recorded the increased fluxes of ions as having energies between 100 and 1000 eV (not shown). These density excursions, in the opposite direction from those observed at Geotail, suggest that rather than Cluster-1 and -4 encountering a perturbed region in the solar wind, the bow shock and magnetosheath moved outward past these two spacecraft during each of these intervals. We note that each of these intervals coincided with one of the magnetic impulses observed on the ground by the IMAGE magnetometer array, and the longest interval of increased density coincided with the magnetic impulse that was accompanied by the Pc 1 wave burst.

[48] As noted in Figure 14, THEMIS A, D, and E were located in the near-equatorial dawn sector outer magnetosphere during this event, near 0700 MLT and at L values increasing from 9.9 at 0900 UT to 11.2 at 1100 UT. Their magnetic footprints mapped west of Greenland, at about 70° MLAT. No significant perturbation of the total magnetic field appeared at these spacecraft between 0900 and 1000 UT (not shown), even during the times Geotail observed the three foreshock structures. They did, however, see a small (~4–6 nT) twist and subsequent relaxation in the magnetic field from 0935 to 0955. The magnetic field perturbations observed at THEMIS A, D, and E at this time, interpreted as field-aligned currents, are consistent with an antisunward-moving TCV in the prenoon sector. These perturbations are thus also consistent with the ground magnetic signatures of a TCV in western Greenland and the ionospheric flow measurements in that same region from the Stokkseyri SuperDARN radar, described in section 4.

7. Discussion

[49] This study began with the presentation of a Pc 1 wave burst that was associated with one of a series of irregular Pc 5 pulses, occurring roughly 1 h after local noon. Both IMAGE magnetometer data (used to display magnetic equivalent convection) and Hankasalmi SuperDARN radar data confirmed that a traveling convection vortex (TCV) was associated with this wave burst, and the radar data confirmed that the TCV was moving eastward (away from local noon). The IMAGE magnetometers detected strong vortical motions from 71.65° to at least 76.43° magnetic latitude (the MLAT of Ny Ålesund, the most poleward station available), and the radar detected strong poleward motions consistent with an azimuthally traveling vortical flow from 76.7° to 78.3° MLAT, in a region of radar backscatter typically associated with the open-closed field line boundary. Close conjunctions of two low-altitude spacecraft (DMSP F17 and NOAA 19) provided additional evidence that the radar-observed traveling vortex was located very near the open-closed field line boundary. Both NOAA 19

proton data and data from a ground-based optical spectrometer showed that proton precipitation occurred over Longyearbyen, suggesting that the Pc 1 wave burst occurred on a flux tube in the outer dayside magnetosphere whose footpoint included Longyearbyen, roughly 2° equatorward of the open-closed field line boundary.

[50] NOAA 19 observations and all-sky auroral images showed additional but less energetic precipitation of both ions and electrons just poleward of the open-closed boundary, indicating the occurrence of a localized dayside reconnection event that occurred simultaneously with the observed TCV and Pc 1 wave burst as well. However, the fact that the Longyearbyen optical spectrometer observed proton precipitation overhead of that site (on closed field lines), along with the observation of more energetic proton precipitation signatures observed by NOAA 19 in that same region, is more consistent with the earlier finding by *Heikkila et al.* [1989], *Yahnin et al.* [1997], and *Moretto and Yahnin* [1998] that TCVs are centered 1° or 2° equatorward of the open-closed boundary.

[51] Auroral imager data also showed the presence of auroral green line (557.7 nm) emissions beginning and ending roughly 2 min earlier than the Pc 1 wave burst and associated proton signature in the Longyearbyen optical spectrometer. We interpreted this time shift as evidence of the difference in travel time of precipitating electrons and protons, consistent with the interpretation of *Zhou et al.* [2009] and the observations of *Ebihara et al.* [2010]. This time shift also makes it possible to reconcile the observations of precipitating energetic protons by NOAA 17 as it passed overhead of Svalbard (0952–0952 UT) with the earlier fading away of the 557.7 nm auroral green line in that region (before 0951).

[52] We have already noted the common near-simultaneous occurrence of TCVs and Pc 1 bursts in very high latitude ground data, as reported by *Arnoldy et al.* [1988, 1996]. Neither of these studies provided information about whether the TCVs and Pc 1 bursts propagated together. *Hughes et al.* [1995], however, presented an example from the MACCS array in Arctic Canada showing that a Pc 1 burst propagated in the same direction as an associated TCV, and *Pilipenko et al.* [1999] presented an example of coordinated motion of a TCV and an associated Pc 1 burst at its leading edge across five longitudinally spaced cusp-latitude MACCS stations. Although the radar data show that the TCV event presented here is similar in its azimuthal motion to these other events, the available magnetometer data are insufficient to demonstrate that the Pc 1 burst traveled with the TCV: both the highest-latitude stations of the IMAGE magnetometer array and the Svalbard search coil magnetometers have very little longitudinal spread, and we are not aware of the existence of any search coil magnetometers at similar magnetic latitudes toward the east. Magnetometer and SuperDARN radar observations in western Greenland also showed the near-simultaneous presence of a TCV in the dawn sector. In this case the Pc 1 signal was detected (with very small amplitude) by only one of the two available search coil magnetometers, both at lower latitudes, so again no conclusion can be drawn about their relative propagation.

[53] As an alternative to the interpretation of TCV-associated Pc 1 bursts as EMIC waves generated near the

equator, *Pilipenko et al.* [1999] proposed that the TCV-associated FAC might be strong enough to cause the occurrence of anomalous resistivity in the upper ionosphere and result in a current instability that would generate the observed Pc 1 waves. The 2 min delay observed during this event between electron precipitation and proton precipitation (and the Pc 1 burst) provides the first direct test of this alternative mechanism, and clearly supports a near-equatorial wave source rather than a local one.

[54] Because many studies, both observational and theoretical, have suggested a causal connection between these phenomena and perturbations at the dayside magnetopause and bow shock, we then focused on the available upstream observations. If dayside reconnection is involved, we would expect to see the presence of a southward-pointing IMF at or shortly before the time of the TCV. If a bow shock related instability was involved, we then would expect to see signatures of such instabilities in data from spacecraft in the solar wind immediately upstream from the bow shock, at or shortly before the time of the TCV, but little or no evidence of such signatures far upstream.

[55] As Figures 15 and 16 show, the time-shifted upstream IMF (observed at ACE, Wind, THEMIS B, and THEMIS C) was oriented predominantly in the Bx direction. Figure 16 shows that the time-shifted Bz component observed by THEMIS B and C was within 1 nT of zero from 0900 to 0940 UT and then increased to near +2 nT during the time of the TCV/Pc 1 burst. The magnetic fields observed by Geotail and Cluster, both just upstream of the dawnside and duskside bow shock, respectively, exhibited positive Bz components throughout the interval from 0900 to 1045 UT. These conditions are clearly not favorable for dayside reconnection, although the precipitation observed just poleward of the open-closed field line boundary is in fact consistent with high latitude reconnection.

[56] What of a bow shock related source? Several different categories of transient kinetic phenomena have been identified upstream of quasi-parallel shocks: HFAs (the first and most commonly observed category of bow shock instability associated with TCVs, discussed in section 6.2); foreshock cavities, cavitons, and bubbles; and most recently SHFAs.

[57] Geotail data (Figure 17) clearly show perturbations in the solar wind upstream of the dawn sector bow shock, but only some of their characteristics were typical for a hot flow anomaly, and they occurred from 15 to 45 min before the TCV/Pc 1 burst event. Three short intervals of reduced and deflected solar wind velocity occurred between 0900 and 0935 UT, and in each of them the ion temperature was greatly increased, and the density was also drastically reduced. The second and third intervals bracketed a ~10 min period of greatly reoriented IMF (between 0921 and 0931 UT), so they are by definition associated with IMF discontinuities, but the first was not, and, inconsistent with our expectations, none of the four upstream solar wind/IMF monitors observed any significant discontinuities during this time interval.

[58] Foreshock cavities, which can result from kinetic interactions between reflected solar wind ions (foreshock ions) and the solar wind, and which need not be associated with IMF discontinuities [*Sibeck et al.*, 2002], are also known to be associated with TCVs. They, however, typically have only minor flow velocity perturbations and

ion temperature increases, features not consistent with the Geotail observations. Foreshock cavitons, with similar magnetic field and plasma characteristics, form as a result of the nonlinear evolution of ULF waves [e.g., *Blanco-Cano et al.*, 2009, 2011], not as a result of IMF discontinuities. Foreshock bubbles, characterized by *Omidi et al.* [2010], also have many of the same observational features, and also have less restrictive requirements for the causative IMF discontinuity. The most recently described category, SHFAs, consists of events similar to HFAs but formed as the result of foreshock cavitons interacting with the bow shock, and again do not require the presence of an IMF discontinuity [*Omidi et al.*, 2013].

[59] The common features of these bow shock related instabilities do appear to fit the three intervals observed in the Geotail data near the bow shock: each exhibits a flow deflection, greatly elevated ion temperatures, greatly reduced ion density, and at least a modest decrease in magnetic field magnitude. The absence of evidence for an IMF discontinuity in upstream data and the plasma characteristics observed at Geotail suggest an SHFA as the most likely candidate to be the driver of the observed TCV/Pc 1 burst.

[60] The simultaneity of the Pc 1 burst observed on the ground 1 h postnoon (~1300 MLT), and the largest outward bow shock excursion observed by Cluster, situated somewhat later in local time (1630 MLT) suggests that these events have a common cause. Although one might consider it paradoxical that a magnetospheric compression can coincide in time with an outward bow shock excursion, both of these features have been seen in other events. *Jacobsen et al.* [2009] reported THEMIS observations of a discontinuity in the solar wind that caused an excursion of the dawn flank magnetopause outward by at least 4.8 R_E that was accompanied by TCV signatures in the Canadian sector. *Korotova et al.* [2012] showed a similar example of a transient magnetospheric compression event characterized by both inward magnetopause motion and outward bow shock motion, triggered by the interaction of an IMF tangential discontinuity with the bow shock. During that event increases in magnetic field strength were observed by GOES 11 and 12 and THEMIS A, D, and E, all located in the outer dayside magnetosphere, while the bow shock moved outward past THEMIS B and C, both located on the dawn flank upstream of the undisturbed bow shock. In addition, *Korotova et al.* [2012] modeled this event using a global hybrid code, which successfully reproduced this seemingly contradictory behavior: The arrival of the discontinuity caused the bow shock to transition from quasi-parallel to quasi-perpendicular, launched a narrow density front into the magnetosheath that briefly compressed the magnetosphere, and initiated outward bow shock motion. Although as noted above no tangential discontinuity was evident in any upstream IMF monitor during the event presented in this paper, both Geotail and Cluster observed short intervals of IMF rotation before and/or during the TCV event that would cause a transition of the subsolar bow shock from quasi-parallel to quasi-perpendicular.

[61] The timing of the observed perturbations at Geotail, however, presents additional difficulties, because the three HFA-like features, separated by ~15 and ~12 min, occurred from 15 to 45 min before the TCV/Pc 1 burst, and the relative timing of these three features does not match well

with the relative timing of the three bow shock excursions past Cluster (separated by ~20 and 35 min, respectively). The positive V_y component of the solar wind velocity observed at Geotail during the 10 min interval between 0921 and 0931 UT does, however, suggest the possibility of propagation, with a reasonable time delay, from the dawnside of the nose of the bow shock to the duskside.

[62] By determining the normal direction to the IMF discontinuity near 0921 UT, **n**, we may be able to estimate the propagation time of this rotation from the location of Geotail to the location of Cluster as $\Delta \mathbf{R} \cdot \mathbf{n} / \mathbf{V}_{sw} \cdot \mathbf{n}$, where $\Delta \mathbf{R}$ is the displacement from Geotail to Cluster. Using the three-point formula for an ideal 1-D transition layer outlined in *Sonnerup and Scheible* [1998] to calculate the normal to the boundary between the plasma regimes before and after 0920 UT seen in the Geotail data (using data at 0910, 0918, and 0925 UT), we obtained a unit vector $\mathbf{n} = (-0.35)$ **i** $+ (0.91)$ **j** $+ (0.22)$ **k**, i.e., predominantly duskward, with a resulting time delay of 17 min, slightly lower than the observed time delay of ~27 min. Using instead a full minimum variance calculation on Geotail IMF data from 0910 to 0925 UT, we found $\mathbf{n} = (-0.13)$ **i** $+ (0.945)$ **j** $+ (0.30)$ **k**, and obtained a resulting time delay of 37 min. (The ratio of eigenvalues of the intermediate and minimum variance directions, $\lambda_{int} / \lambda_{min} = 2.64$, is greater than the threshold of 1.5 for the condition of suitability of the minimum variance method [*Sonnerup and Cahill*, 1967].)

[63] Although these two methods give time delays that bracket the observed time delay, they do so with differences of $> \pm 35\%$. We point out that it is more likely that the bow shock instability was located nearer the nose of the bow shock and propagated both dawnward (to Geotail) and duskward (to Cluster). Because no spacecraft were positioned near the nose, however, the above numerical estimates are at best only suggestive of possible causal relations, and our understanding of the detailed connections between the variations observed at Geotail, Cluster, and on Svalbard must remain inconclusive.

[64] Finally, one might wonder whether there is truly a causal connection between the spontaneous hot flow anomaly observed by satellites in the Southern Hemisphere and the TCV and Pc1 burst observed in the Northern Hemisphere. Earlier multistation studies have shown similar TCV behavior in ground magnetometer data at both ends of a dayside flux tube [*Kataoka et al.*, 2001; *Murr et al.*, 2002]. Pc1 waves have similarly been observed at ground stations in both hemispheres [*Arnoldy et al.*, 1988, 1996]. *Engebretson et al.* [2002] observed Pc 1 waves (not wave bursts, but associated with longer-lasting compressions) in data from the Polar satellite in the Northern Hemisphere and simultaneously in data from Antarctic ground stations. These studies suggest that the EMIC waves and the field-aligned currents associated with the TCV can be observed anywhere along a given flux tube; once generated, both propagate toward both ionospheres. The fact that during this event the satellites in the magnetosheath were in the Southern Hemisphere and the ground stations were in the Northern Hemisphere simply adds more evidence (indirect, at least) that both TCV-related FACs and EMIC waves propagate along the entire flux tube. Our data for this event give us no information on the exact latitude(s) of their

generation, but the data are certainly consistent with a near-equatorial source.

8. Summary and Conclusions

[65] An isolated Pc 1 wave burst was observed roughly 1 h after local noon at four locations in Svalbard, from ~1° to 3° equatorward of the footpoint of the open/closed field line boundary, near the beginning of one of a series of magnetic impulse events. A plot of magnetic equivalent convection showed evidence of up to three vortex events, the second (and largest) being associated with the Pc 1 burst.

[66] Hankasalmi SuperDARN radar data showed eastward (duskward) motion of an ionospheric disturbance near the open-closed field line boundary, confirming that the event was a TCV. A near-simultaneous TCV was observed over western Greenland in ground magnetometer and Stokkseyri SuperDARN radar data, demonstrating that the TCV was extended also to the prenoon sector. However, the limited number of stations in the longitudinal direction did not allow us to observe possible longitudinal variations of the TCV.

[67] Precipitating protons were detected on the flux tube above Longyearbyen by a ground-based optical spectrometer, in good temporal agreement with the observed Pc 1 wave burst. NOAA 19 satellite data also detected precipitating protons of ring current energies during its pass just west of Svalbard during the time of the Pc 1 burst. These observations confirm that compression-related EMIC waves can be generated very near the outer boundary of the dayside magnetosphere, consistent with the event study of *Anderson et al.* [1996] and with the statistical studies of AMPTE CCE data [*Anderson et al.*, 1992] and THEMIS data [*Usanova et al.*, 2012] showing that the dayside outer magnetosphere is a preferential location for EMIC activity, with the occurrence rate being strongly controlled by solar wind dynamic pressure.

[68] Although data from several upstream spacecraft showed a rather steady IMF before and during this event, IMF data from Geotail and Cluster near the bow shock showed considerable temporal structure, suggesting that a bow shock related instability, observed by Geotail on the dawn flank, may have been responsible for both this TCV/ Pc 1 burst event and the nearly simultaneous outward excursion of the afternoon sector bow shock observed by Cluster. Of the categories of bow shock related instabilities currently identified, an SHFA best fits the available observations.

[69] This study brings together data from a variety of instruments to expand some aspects of our knowledge of TCV/Pc 1 burst events. Simultaneous overflights of two low-altitude spacecraft, along with SuperDARN radar data, have made it possible to not only determine the location of this event to be at a magnetic latitude very near to the open-closed boundary of the postnoon dayside magnetosphere, but also to characterize the energy of the proton precipitation associated with the observed proton aurora and EMIC waves. Thus, for the first time we have observed a clear temporal association between auroral proton emissions and the appearance of EMIC waves in ground magnetometer data within 1° to 3° of the open-closed field line boundary, and both in association with a TCV event

[70] This study also adds to the number of magnetospheric compression events simultaneous with large outward flank

bow shock excursions. The results of the global hybrid modeling reported by *Korotova et al.* [2012] appear to reconcile the apparent contradiction between compression of the dayside magnetosphere (inward motion of the dayside magnetopause) and outward motion of the flank bow shock. We thus do not need to postulate a new mechanism for the generation of Pc 1 bursts in association with TCVs. The ability of the EMIC instability to generate such bursts, stimulated by the rapid, transient compression of a marginally unstable pitch angle distribution of energetic ions in the outer magnetosphere, is strongly supported by the observation of simultaneous, spatially localized precipitation of 30 to 250 keV protons.

[71] The available data, however, are insufficient to address two other issues related to TCV/Pc 1 burst events. First, the available ground observations of Pc 1 burst do not provide the longitudinal spacing of stations needed to determine whether the TCV and Pc 1 burst propagated together in longitude, as was the case in the event shown by *Pilipenko et al.* [1999]. Second, although the upstream IMF and plasma data strongly suggest that an SHFA may be the cause of the perturbations that produced the TCV and Pc 1 burst reported here, the limited number of spacecraft observations, and their locations quite far from the subsolar bow shock, prevents a more detailed characterization of that bow shock related phenomenon. Further multipoint studies of such events, with even more favorable alignments of ground-based and satellite instrumentation, will be needed to address these issues.

References

Anderson, B. J., and D. C. Hamilton (1993), Electromagnetic ion cyclotron waves stimulated by modest magnetospheric compressions, *J. Geophys. Res.*, *98*, 11,369–11,382, doi:10.1029/93JA00605.

Anderson, B. J., R. E. Erlandson, and L. J. Zanetti (1992), A statistical study of Pc 1–2 magnetic pulsations in the equatorial magnetosphere: 1. Equatorial occurrence distributions, *J. Geophys. Res.*, *97*, 3075–3088, doi:10.1029/91JA02706.

Anderson, B. J., R. E. Erlandson, M. J. Engebretson, J. L. Alford, and R. L. Arnoldy (1996), Source region of 0.2 to 1.0 Hz geomagnetic pulsation bursts, *Geophys. Res. Lett.*, *23*, 769–772, doi:10.1029/96GL00659.

Archer, M. O., T. S. Horbury, and J. P. Eastwood (2012), Magnetosheath pressure pulses: Generation downstream of the bow shock from solar wind discontinuities, *J. Geophys. Res.*, *117*, A05228, doi:10.1029/2011JA017468.

Arnoldy, R. L., M. J. Engebretson, and L. J. Cahill Jr. (1988), Bursts of Pc 1-2 near the ionospheric footprint of the cusp and their relationship to flux transfer events, *J. Geophys. Res.*, *93*, 1007–1016.

Arnoldy, R. L., M. J. Engebretson, J. L. Alford, R. E. Erlandson, and B. J. Anderson (1996), Magnetic impulse events and associated Pc 1 bursts at dayside high latitudes, *J. Geophys. Res.*, *101*, 7793–7799.

Arnoldy, R. L., et al. (2005), Pc 1 waves and associated unstable distributions of magnetospheric protons observed during a solar wind pressure pulse, *J. Geophys. Res.*, *110*, A07229, doi:10.1029/2005JA011041.

Baker, K. B., J. R. Dudeney, R. A. Greenwald, M. Pinnock, P. T. Newell, A. S. Rodger, N. Mattin, and C. I. Meng (1995), HF radar signatures of the cusp and low-latitude boundary layer, *J. Geophys. Res.*, *100*, 7671–7695, doi:10.1029/94JA01481.

Blanco-Cano, X., N. Omidi, and C. T. Russell (2009), Global hybrid simulations: Foreshock waves and cavitons under radial interplanetary magnetic field geometry, *J. Geophys. Res.*, *114*, A01216, doi:10.1029/2008JA013406.

Blanco-Cano, X., P. Kajdič, N. Omidi, and C. T. Russell (2011), Foreshock cavitons for different interplanetary magnetic field geometries: Simulations and observations, *J. Geophys. Res.*, *116*, A09101, doi:10.1029/2010JA016413.

Bolshakova, O. V., and V. A. Troitskaya (1982), Impulse reconnection as a possible source of ipcl pulsations, *Geomag. Aeron.*, *22*, 877.

Bolshakova, O. V., N. G. Kleimenova, and N. A. Kurazhkovskaya (1988), Polar cap dynamics using the observations of long period geomagnetic pulsations, *Geomag. Aeron.*, *28*, 661.

Chaston, C. C., et al. (2005) Drift kinetic Alfvén waves observed near a reconnection X line in the Earth's magnetopause, *Phys. Rev. Lett.*, *95*, 065002, doi:10.1103/Phys.Rev. Lett. 95.065002.

Chisham, G., and M. P. Freeman (2003), A technique for accurately determining the cusp-region polar cap boundary using SuperDARN HF radar measurements, *Ann. Geophys.*, *21*, 983–996, doi:10.5194/angeo-21-983-2003.

Chisham, G., et al. (2007), A decade of the Super Dual Auroral Radar Network (SuperDARN): Scientific achievements, new techniques and future directions, *Surv. Geophys.*, *28*, 33–109, doi:10.1007/s10712-007-9017-8.

Chisham, G., T. Yeoman, and G. J. Sofko (2008), Mapping ionospheric backscatter measured by the SuperDARN HF radars - part 1: A new empirical virtual height model, *Ann. Geophys.*, *26*, 823–841, doi:10.5194/angeo-26-823-2008.

Clausen, L. B. N., J. B. H. Baker, J. M. Ruohoniemi, and H. J. Singer (2011), EMIC waves observed at geosynchronous orbit during solar minimum: Statistics and excitation, *J. Geophys. Res.*, *116*, A10205, doi:10.1029/2011JA016823.

Cowley, S. W. H. (2000), Magnetosphere-ionosphere interactions: A tutorial review, in *Magnetospheric Current Systems, Geophys. Monogr. Ser.*, vol. 118, edited by S. Ohtani et al., pp. 91–106, AGU, Washington, D. C., doi:10.1029/GM118p0091.

Eastwood, J. P., et al. (2008), THEMIS observations of a hot flow anomaly: Solar wind, magnetosheath, and ground-based measurements, *Geophys. Res. Lett.*, *35*, L17S03, doi:10.1029/2008GL033475.

Ebihara, Y., R. Kataoka, A. T. Weatherwax, and M. Yamauchi (2010), Dayside proton aurora associated with magnetic impulse events: South Pole observations, *J. Geophys. Res.*, *115*, A04301, doi:10.1029/2009JA014760.

Engebretson, M. J., W. K. Peterson, J. L. Posch, M. R. Klatt, B. J. Anderson, C. T. Russell, H. J. Singer, R. L. Arnoldy, and H. Fukunishi (2002), Observations of two types of Pc 1-2 pulsations in the outer dayside magnetosphere, *J. Geophys. Res.*, *107* (A12), 1451, doi:10.1029/2001JA000198.

Engebretson, M. J., J. Moen, J. L. Posch, F. Lu, M. R. Lessard, H. Kim, and D. A. Lorentzen (2009), Searching for ULF signatures of the cusp: Observations from search coil magnetometers and auroral imagers in Svalbard, *J. Geophys. Res.*, *114*, A06217, doi:10.1029/2009JA014278.

Evans, D. S., and M. S. Greer (2000), *Polar orbiting environmental satellite space environment monitor - 2: Instrument descriptions and archive data documentation, NOAA Technical Memorandum OAR SEC-93*, NOAA Space Environment Center, Boulder, Colo.

Friis-Christensen, E., M. A. McHenry, C. R. Clauer, and S. Vennerstrøm (1988), Ionospheric traveling convection vortices observed near the polar cleft: A triggered response to sudden changes in the solar wind, *Geophys. Res. Lett.*, 15(3), 253.

Glassmeier, K.-. H., M. Hönisch, and J. Untiedt (1989), Ground-Based and Satellite Observations of Traveling Magnetospheric Convection Twin Vortices, *J. Geophys. Res.*, 94, 2520–2528.

Greenwald, R. A., et al. (1995), DARN/SuperDARN a global view of the dynamics of high latitude convection, *Space Sci. Rev.*, 71, 761–796, doi:10.1007/BF00751350.

Heikkila, W. J., T. S. Jorgensen, L. J. Lanzerotti, and C. G. Maclennan (1989), A transient auroral event on the dayside, *J. Geophys. Res.*, 94, 15,291–15,305, doi:10.1029/JA094iA11p15291.

Hughes, W. J., M. J. Engebretson, and E. Zesta (1995), Ground observations of transient cusp phenomena: Initial results from MACCS, in *Physics of the Magnetopause*, Geophysical Monograph Series 90, edited by P. Song, B. U. O. Sonnerup, and M. F. Thomsen, pp. 427–437, AGU, Washington, D.C.

Immel, T. J., S. B. Mende, H. U. Frey, J. Patel, J. W. Bonnell, M. J. Engebretson, and S. A. Fuselier (2005), ULF waves associated with enhanced subauroral proton precipitation, in *Inner Magnetosphere Interactions: New Perspectives from Imaging*, Geophysical Monograph Series 159, edited by J. Burch, M. Schulz, and H. Spence, pp. 71–84, AGU, Washington, D.C., doi:10.1029/159GM05.

Ishida, J., S. Kokubun, and R. L. McPherron (1987), Substorm effects on spectra structures of Pc 1 waves at synchronous orbit, *J. Geophys. Res.*, 92, 143–158.

Jacobsen, K. S., et al. (2009), THEMIS observations of extreme magnetopause motion caused by a hot flow anomaly, *J. Geophys. Res.*, 114, A08210, doi:10.1029/2008JA013873.

Kangas, J., A. Aikio, and J. V. Olson (1986), Multistation correlation spectra associated with sudden impulses, *Planet. Space Sci.*, 34, 543–553.

Kangas, J., A. Guglielmi, and O. Pokhotelov (1998), Morphology and physics of short-period geomagnetic pulsations, *Space. Sci. Rev.*, 83, 435–512, doi:10.1023/A:1005063911643.

Kataoka, R., H. Fukunishi, L. J. Lanzerotti, C. G. Aclennan, H. U. Frey, S. B. Mende, J. H. Doolittle, T. J. Rosenberg, and A. T. Weatherwax (2001), Magnetic impulse event: A detailed case study of extended ground and space observations, *J. Geophys. Res.*, 106, 25873–25889, doi:10.1029/2000JA000314.

Kataoka, R., H. Fukunishi, and L. J. Lanzerotti (2003), Statistical identification of solar wind origins of magnetic impulse events, *J. Geophys. Res.*, 108(A12), 1436, doi:10.1029/2003JA010202.

Kleimenova, N. G., O. V. Bolshakova, V. A. Troitskaya, and E. Friis-Christensen (1985), Two types of long period geomagnetic pulsations near equator border of dayside polar cusp, *Geomag. Aeron.*, 25, 163.

Konik, R. M., L. J. Lanzerotti, A. Wolfe, C. G. Maclennan, and D. Venkatesan (1994), Cusp latitude magnetic impulse events: 2. Interplanetary magnetic field and solar wind conditions, *J. Geophys. Res.*, 99(A8), 14,831–14,853, doi:10.1029/93JA03241.

Korotova, G. I., D. G. Sibeck, N. Omidi, and V. Angelopoulos (2012), THEMIS observations of unusual bow shock motion attending a transient magnetospheric event, *J. Geophys. Res.*, 117, A12207, doi:10.1029/2012JA017510.

Kurazkovskaya, N. A., and B. I. Klain (2000), Peculiar features of burst series of long-period irregular IPCL-type geomagnetic pulsations in the vicinity of the dayside cusp, *Geomagn. Aeronomy International*, 2, 129–135.

Lester, M., et al. (2004), Stereo CUTLASS - a new capability for the SuperDARN HF radars, *Ann. Geophys.*, 22, 459–473, doi:10.5194/angeo-22-459-2004.

Lockwood, M., and J. Moen (1996), Ion populations on open field lines within the dayside low-latitude boundary Layer: Theory and observations during a transient event, *Geophys. Res. Lett.*, 23(21), 2895–2898.

Lockwood, M., S. W. H. Cowley, P. E. Sandholt, and R. P. Lepping (1990), The Ionospheric Signatures of Flux Transfer Events and Solar Wind Dynamic Pressure Changes, *J. Geophys. Res.*, 95(A10), 17,113–17,135, doi:10.1029/JA095iA10p17113.

Lorentzen, D. A., C. S. Deehr, J. I. Minow, R. W. Smith, H. C. Stenbaek-Neielsen, F. Sigernes, R. L. Arnoldy, and K. Lynch (1996), SCIFER-Dayside auroral signatures of magnetospheric energetic electrons, *Geophys. Res. Lett.*, 23, 1885–1888, doi:10.1029/96GL00593.

Lorentzen, D. A., and J. Moen (2000), Auroral proton and electron signatures in the dayside aurora, *J. Geophys. Res.*, 105, 12,733–12,745, doi:10.1029/1999JA900405.

Lühr, H. and W. Blawert (1994), Ground signatures of travelling convection vortices, in *Solar Wind Sources of Magnetospheric Ultra-Low-Frequency Waves*, Geophys. Monogr. Ser., vol. 81, edited by M. J. Engebretson, K. Takahashi, and M. Scholer, pp. 231–251, AGU, Washington, D.C.

McCollough, J. P., S. R. Elkington, and D. N. Baker (2012), The role of Shabansky orbits in compression-related electromagnetic ion cyclotron wave growth, *J. Geophys. Res.*, 117, A01208, doi:10.1029/2011JA016948.

McHenry, M. A., C. R. Clauer, and E. Friis-Christensen (1990), Relationship of solar wind parameters to continuous, dayside high latitude traveling ionospheric convection vortices, *J. Geophys. Res.*, 95, 15007–15022.

Moen, J., P. E. Sandholt, M. Lockwood, W. F. Denig, U. P. Løvhaug, B. Lybekk, A. Egeland, D. Opsvik, and E. Friis-Christensen (1995), Events of enhanced convection and related dayside auroral activity, *J. Geophys. Res.*, 100, 23,917–23,934, doi:10.1029/95JA02585.

Moen, J., D. Evans, H. C. Carlson, and M. Lockwood (1996), Dayside moving auroral transients related to LLBL dynamics, *Geophys. Res. Lett.*, 23(22), 3247–3250.

Moen, J., D. A. Lorentzen, and F. Sigernes (1998), Dayside moving auroral forms and bursty proton auroral events in relation to particle boundaries observed by NOAA 12, *J. Geophys. Res.*, 103, 14,855–14,863, doi:10.1029/97JA02877.

Moen, J., H. C. Carlson, S. E. Milan, N. Shumilov, B. Lybekk, P. E. Sandholt, and M. Lester (2000), On the collocation between dayside auroral activity and coherent HF radar backscatter, *Ann. Geophys.*, 18, 1531–1549.

Moretto, T., and A. Yahnin (1998), Mapping travelling convection vortex events with respect to energetic particle boundaries, *Ann. Geophys.*, 16, 891.

Murr, D. L., W. J. Hughes, A. S. Rodger, E. Zesta, H. U. Frey, and A. T. Weatherwax (2002), Conjugate observations of traveling convection vortices: The field-aligned current system, *J. Geophys. Res.*, 107(A10), 1306, doi:10.1029/2002JA009456.

Murr, D. L., and W. J. Hughes (2003), Solar wind drivers of Traveling Convection Vortices, *Geophys. Res. Lett.*, 30(7), 1354, doi:10.1029/2002GL015498.

Nomura, R., K. Shiokawa, K. Sakaguchi, Y. Otsuka, and M. Connors (2012), Polarization of Pc1/EMIC waves and related proton auroras observed at subauroral latitudes, *J. Geophys. Res.*, 117, A02318, doi:10.1029/2011JA017241.

Oksavik, K., F. Søraas, J. Moen, and W. J. Burke (2000), Optical and particle signatures of magnetospheric boundary layers near magnetic noon: Satellite and ground-based observations, *J. Geophys. Res.*, 105, 27,555–27,568.

Oksavik, K., F. Søraas, J. Moen, R. Pfaff, J. A. Davies, and M. Lester (2004), Simultaneous optical, CUTLASS HF radar, and FAST spacecraft observations: Signatures of boundary layer processes in the cusp, *Ann. Geophys.*, 22, 511–525.

Olson, J. V., and L. C. Lee (1983), Pc 1 wave generation by sudden impulses, *Planet. Space Sci.*, 31, 295–302.

Omidi, N., J. P. Eastwood, and D. G. Sibeck (2010), Foreshock bubbles and their global magnetospheric impacts, *J. Geophys. Res.*, 115, A06204, doi:10.1029/2009JA014828.

Omidi, N., H. Zhang, D. Sibeck, and D. Turner (2013), Spontaneous hot flow anomalies at quasi-parallel shocks, 2, Hybrid simulations, *J. Geophys. Res. Space Physics*, 118, 173–180, doi:10.1029/2012JA018099.

Pilipenko, V. A., S. L. Shalimov, E. N. Fedorov, M. J. Engebretson, and W. J. Hughes (1999), Coupling between field-aligned current impulses and Pi1 noise bursts, *J. Geophys. Res.*, 104, 17,419–17,430, doi:10.1029/1999JA900190.

Posch, J. L., M. J. Engebretson, M. T. Murphy, M. H. Denton, M. R. Lessard, and R. B. Horne (2010), Probing the relationship between EMIC waves and plasmaspheric plumes near geosynchronous orbit, *J. Geophys. Res.* 115, A11205, doi:10.1029/2010JA015446.

Posch, J. L., M. J. Engebretson, M. R. Lessard, D. L. Murr, H. J. Singer, T. Raita, and A.J. Witte (2011), Simultaneous Traveling Convection Vortex (TCV) Events and Pc 1-2 Wave Bursts at Cusp/Cleft Latitudes, presented at the 2011 CEDAR/GEM Workshops, Santa Fe, NM, June 28, 2011.

Sakaguchi, K., K. Shiokawa, A. Ieda, Y. Miyoshi, Y. Otsuka, T. Ogawa, M. Connors, E. F. Donovan, and F. J. Rich (2007), Simultaneous ground and satellite observations of an isolated proton arc at subauroral latitudes, *J. Geophys. Res.*, 112, A04202, doi:10.1029/2006JA012135.

Sakaguchi, K., K. Shiokawa, Y. Miyoshi, Y. Otsuka, T. Ogawa, K. Asamura, and M. Connors (2008), Simultaneous appearance of isolated auroral arcs and Pc 1 geomagnetic pulsations at subauroral latitudes, *J. Geophys. Res.*, 113, A05201, doi:10.1029/2007JA012888.

Sandanger, M., F. Søraas, K. Aarsnes, K. Oksavik, and D. S. Evans (2007), Loss of relativistic electrons: Evidence for pitch angle scattering by electromagnetic ion cyclotron waves excited by unstable ring current protons, *J. Geophys. Res.*, 112, A12213, doi:10.1029/2006JA012138.

Sandholt, P. E., C. J. Farrugia, J. Moen, Ø. Noraberg, B. Lybekk, T. Sten, and T. L. Hansen (1998), A classification of dayside auroral forms and

activities as a function of interplanetary magnetic field orientation, *J. Geophys. Res.*, *103*, 23,325–23,345, doi:10.1029/98JA02156.

Sergeev, V. A., E. M. Sazhina, N. A. Tsyganenko, J. Å. Lundblad, and F. Søraas (1983), Pitch-angle scattering of energetic protons in the magnetotail current sheet as the dominant source of their isotropic precipitation into the nightside ionosphere, *Planet. Space Sci.*, *31*, 1147–1155.

Sibeck, D., et al. (1999), Comprehensive study of the magnetospheric response to a hot flow anomaly, *J. Geophys. Res.*, *104*, 4577–4593.

Sibeck, D. G., R. W. McEntire, A. T. Y. Lui, R. E. Lopez, and S. M. Krimigis (1987), Magnetic field drift shell splitting: Cause of unusual dayside particle pitch angle distributions during storms and substorms, *J. Geophys. Res.*, *92*, 13,485–13,497, doi:10.1029/JA092iA12p13485.

Sibeck, D. G., T.-D. Phan, R. Lin, R. P. Lepping, and A. Szabo (2002), Wind observations of foreshock cavities: A case study, *J. Geophys. Res.*, *107*(A10), 1271, doi:10.1029/2001JA007539.

Smets, R., D. Delcourt, J. A. Sauvaud, and P. Koperski (1999), Electron pitch angle distributions following the dipolarization phase of a substorm: Interball-Tail observations and modeling, *J. Geophys. Res.*, *104*, 14571–14581.

Sonnerup, B. U. Ö., and L. J. Cahill Jr. (1967), Magnetopause structure and attitude from Explorer 12 observations, *J. Geophys. Res.*, *72*, 171–183, doi:10.1029/JZ072i001p00171.

Sonnerup, B. U. Ö., and M. Scheible (1998), Minimum and maximum variance analysis, in *Analysis Methods for Multi-Spacecraft Data, ISSI Scientific Rep. SR-001*, edited by G. Paschmann and P. W. Daly, pp. 185–220, Eur. Space Agencey Publ. Div., Noordwijk, Netherlands.

Stasiewicz, K., C. E. Seyler, F. S. Mozer, G. Gustafsson, J. Pickett, and B. Popielawska (2001), Magnetic bubbles and kinetic Alfvén waves in the high-latitude magnetopause boundary, *J. Geophys. Res.*, *106*, 29,503–29,514, doi:10.1029/2001JA900055.

Thomsen, M. F., J. T. Gosling, S. A. Fuselier, S. J. Bame, and C. T. Russell (1986), Hot, diamagnetic cavities upstream from the Earth's bow shock, *J. Geophys. Res.*, *91*, 2961–2973.

Turner, D. L., S. Eriksson, T. D. Phan, V. Angelopoulos, W. Tu, W. Liu, X. Li, W.-L. Teh, J. P. McFadden, and K.-H. Glassmeier (2011), Multispacecraft observations of a foreshock-induced magnetopause disturbance exhibiting distinct plasma flows and an intense density compression, *J. Geophys. Res.*, *116*, A04230, doi:10.1029/2010JA015668.

Urban, K. D., A. J. Gerrard, Y. Bhattacharya, A. J. Ridley, L. J. Lanzerotti, and A. T. Weatherwax (2011), Quiet time observations of the open-closed boundary prior to the CIR-induced storm of 9 August 2008, *Space Weather*, *9*, S11001, doi:10.1029/2011SW000688.

Usanova, M. E., I. R. Mann, I. J. Rae, Z. C. Kale, V. Angelopoulos, J. W. Bonnell, K. H. Glassmeier, H. U. Auster, and H. J. Singer (2008), Multipoint observations of magnetic compression-related EMIC Pc1 waves by THEMIS and CARISMA, *Geophys. Res. Lett.*, *35*, L17S25, doi:10.1029/2008GL034458.

Usanova, M. E., et al. (2010), Conjugate ground and multisatellite observations of compression-related EMIC Pc1 waves and associated proton precipitation, *J. Geophys. Res.*, *115*, A07208, doi:10.1029/2009JA014935.

Usanova, M. E., I. R. Mann, J. Bortnik, L. Shao, and V. Angelopoulos (2012), THEMIS observations of electromagnetic ion cyclotron wave occurrence: Dependence on AE, SYMH, and solar wind dynamic pressure, *J. Geophys. Res.*, *117*, A10218, doi:10.1029/2012JA018049.

Villain, J. P., R. André, M. Pinnock, R. A. Greenwald, and C. Hanuise (2002), A statistical study of the Doppler spectral width of high-latitude ionospheric F-region echoes recorded with SuperDARN coherent HF radars, *Ann. Geophys.*, *20*, 1769–1781, doi:10.5194/angeo-20-1769-2002.

Wu, P., T. A. Fritz, B. Lavraud, and E. Lucek (2006), Substorm associated magnetotail energetic electrons pitch angle evolutions and flow reversals: Cluster observation, *Geophys. Res. Lett.*, *33*, L17101, doi:10.1029/2006GL026595.

Yahnin, A. G., and T. A. Yahnina (2007), Energetic proton precipitation related to ion-cyclotron waves, *J. Atmos. Solar-Terr. Phys.*, *69*, 1690–1706.

Yahnin, A. G., T. A. Yahnina, and H. U. Frey (2007), Subauroral proton spots visualize the Pc1 source, *J. Geophys. Res.*, *112*, A10223, doi:10.1029/2007JA012501.

Yahnina, T. A., A. G. Yahnin, J. Kangas, and J. Manninen (2000), Proton precipitation related to Pc1 pulsations, *Geophys. Res. Lett.*, *27*, 3575–3578, doi:10.1029/2000GL003763.

Yeoman, T. K., D. M. Wright, A. J. Stocker, and T. B. Jones (2001), An evaluation of range accuracy in the SuperDARN over-the-horizon HF radar systems, *Radio Sci.*, *36*, 801–813, doi:10.1029/2000RS002558.

Yeoman, T. K., G. Chisham, L. J. Baddeley, R. S. Dhillon, T. J. T. Karhunen, T. R. Robinson, A. Senior, and D. M. Wright (2008), Mapping ionospheric backscatter measured by the SuperDARN HF radars - part 2: Assessing SuperDARN virtual height models, *Ann. Geophys.*, *26*, 843–852, doi:10.5194/angeo-26-843-2008.

Zhou, X.-Y., K. Fukui, H. C. Carlson, J. I. Moen, and R. J. Strangeway (2009), Shock aurora: Ground-based imager observations, *J. Geophys. Res.*, *114*, A12216, doi:10.1029/2009JA014186.

Zolotukhina, N., V. Pilipenko, M. J. Engebretson, and A. S. Rodger (2007), Response of the inner and outer magnetosphere to solar wind density fluctuations during the recovery phase of a moderate magnetic storm, *J. Atmos. Solar Terr. Phys.*, *69*, 1707–1722.